Research Square

Preprints are preliminary reports that have not undergone peer review.
They should not be considered conclusive, used to inform clinical practice,
or referenced by the media as validated information.

Genomic characterization of aminoglycoside resistance mechanisms using third generation nanopore sequencing without polymerase chain reaction in Egyptian primary healthcare centers

Mohammed Kassab

mohammed.kassab@pharma.cu.edu.eg

Cairo University

Research Article

Keywords: Aminoglycoside resistance, Third-generation sequencing, Nanopore, Primary healthcare, Egypt, AMR genomics, PCR-free diagnostics

Posted Date: November 25th, 2026

DOI: https://doi.org/10.21203/rs.3.rs-11728163/v1

License: This work is licensed under a Creative Commons Attribution 4.0 International License.
Read Full License

Additional Declarations: No competing interests reported.

Genomic characterization of aminoglycoside resistance mechanisms using third generation nanopore sequencing without polymerase chain reaction in Egyptian primary healthcare centers

Prof. Dr. Mohammed Kassab

Department of Microbiology and Immunology, Faculty of Pharmacy, Cairo University, Cairo, Egypt

Email: mohammed.kassab@pharma.cu.edu.eg; ksabmhmd676@gmail.com | ORCID: 0000-0003-2554-0663

Abstract

Background: Aminoglycoside antibiotics are essential for treating severe Gram-negative infections in Egyptian primary healthcare centers (PHCs), yet resistance rates have escalated substantially. Traditional molecular detection methods, including PCR and 16S rRNA sequencing, are impractical in resource-limited PHC settings due to cost, infrastructure constraints, and dependency on prior sequence knowledge. Third-generation nanopore sequencing offers a PCR-free, hypothesis-independent platform capable of simultaneously resolving species identity, resistance determinants, and mobile genetic architecture from a single sequencing run.

Objective: To characterize the genomic mechanisms of aminoglycoside resistance among bacterial isolates from Egyptian PHC patients using Oxford Nanopore whole-genome sequencing exclusively, without reliance on PCR or 16S rRNA sequencing methodologies.

Methods: Clinical isolates were collected from patients with respiratory tract, urinary tract, and wound infections across PHCs in three Egyptian governorates. Phenotypic resistance was confirmed by broth microdilution for gentamicin, tobramycin, amikacin, and kanamycin. High-molecular-weight DNA was sequenced on Oxford Nanopore platforms using rapid barcoding chemistry without PCR amplification. Species identification employed whole-genome Mash and FastANI comparison. Resistance gene detection utilized CARD and ResFinder databases. Chromosomal mutations in efflux pump regulators and 16S rRNA genes were identified through reference-based variant calling. Mobile genetic elements were characterized using PlasmidFinder and ISfinder.

Results: A total of 247 Gram-negative isolates were sequenced to a mean coverage depth of 62× (range: 48–89×). The predominant species were Klebsiella pneumoniae (85/247, 34.4%), Escherichia coli (65/247, 26.3%), Pseudomonas aeruginosa (48/247, 19.4%), and Acinetobacter baumannii (31/247, 12.6%). Phenotypic aminoglycoside resistance was detected in 177/247 isolates (71.7%). The most prevalent aminoglycoside-modifying enzyme genes were aac(6')-Ib (144/247, 58.3%), aadA2 (117/247, 47.4%), aph(3")-Ia (95/247, 38.5%), aac(3)-IIa (79/247, 32.0%), and ant(2")-Ia (55/247, 22.3%). The 16S rRNA methyltransferase gene armA was identified in 36/247 isolates (14.6%), predominantly in A. baumannii (20/31, 64.5%) and K. pneumoniae (16/85, 18.8%). The rmtB gene was detected in 7/247 isolates (2.8%), exclusively in K. pneumoniae (7/85, 8.2%). Chromosomal mutations in efflux pump regulatory genes were identified in 102/247 isolates (41.3%), with acrR mutations in 56/247 (22.7%), marR in 39/247 (15.8%), and soxR in 24/247 (9.7%). Long-read sequencing revealed that 169/247 resistance genes (68.4%) were physically linked to mobile genetic elements, including IS26 (102/247, 41.3%), class 1 integrons (83/247, 33.6%), and ISCR1 (45/247, 18.2%). Plasmid-mediated resistance was

identified in 135/247 isolates (54.7%), predominantly associated with IncF (52/135, 38.5%), IncX3 (32/135, 23.7%), and IncA/C (20/135, 14.8%) replicon types. Regional analysis demonstrated significantly higher armA prevalence in Upper Egypt (24/104, 23.1%) compared to Lower Egypt (12/143, 8.4%; χ^2 = 9.42, p = 0.002). Genotype–phenotype concordance was 226/247 (91.5%; κ = 0.82, 95% CI: 0.76–0.88).

Conclusions: This study established a fully sequence-based framework for aminoglycoside resistance surveillance in Egyptian PHCs. The high prevalence of aac(6')-Ib (58.3%), aadA2 (47.4%), and aph(3'')-Ia (38.5%), combined with substantial mobile genetic element association (68.4%), indicates extensive horizontal dissemination potential. The identification of armA in 14.6% of isolates raises concerns regarding limited therapeutic alternatives. Nanopore sequencing successfully resolved resistance mechanisms without PCR or 16S rRNA methodologies, demonstrating feasibility for implementation in resource-constrained primary healthcare settings.

Clinical trial number: Not applicable.

Keywords: *Aminoglycoside resistance; Third-generation sequencing; Nanopore; Primary healthcare; Egypt; AMR genomics; PCR-free diagnostics*

Introduction

Aminoglycoside antibiotics, including gentamicin, tobramycin, and amikacin, constitute a cornerstone of empirical therapy for severe Gram-negative infections in Egypt's primary healthcare system. However, aminoglycoside resistance among Egyptian clinical isolates has reached alarming proportions. A cross-sectional study at Fayoum University Surgical Hospital demonstrated that 63.5% of non-fermenting Gram-negative rods were resistant to aminoglycosides, with armA identified in 97.7% of tested isolates (1). In Alexandria, among K. pneumoniae isolates causing respiratory tract infections, 46.67% harbored armA and 50% carried aac(6')-Ib, with all aminoglycoside-resistant isolates classified as multidrug-resistant (2). Among Egyptian A. baumannii isolates, armA co-existed with mphE and msrE on the same resistance island, reflecting the convergence of multiple resistance determinants within single strains (3).

The molecular mechanisms of aminoglycoside resistance are tripartite: enzymatic modification by aminoglycoside-modifying enzymes (AMEs), target site alteration through 16S rRNA methyltransferases or ribosomal mutations, and reduced intracellular accumulation via efflux pump overexpression or porin loss (4). A comprehensive study of P. aeruginosa from Minia hospitals, Egypt, revealed that 94.1% of aminoglycoside-resistant isolates harbored modifying enzyme genes, with aac(6')-Ib being the most prevalent (79.4%), while resistance methyltransferase genes were found in 55.9% of isolates (5). In Egyptian A. baumannii clinical isolates, aph(3')-VIa was identified as a predominant determinant alongside significant up-regulation of AdeABC and AdeKJL efflux pump genes, demonstrating the synergistic contribution of enzymatic modification and reduced drug accumulation (6). Critically, AME genes are frequently mobilized on integrons, transposons, and conjugative plasmids, facilitating horizontal dissemination across species barriers (7).

The 16S rRNA methyltransferases, including armA and rmtA through rmtH, confer high-level resistance to all clinically relevant aminoglycosides by methylating the ribosomal decoding site (8). Efflux pump

systems, particularly the RND family (AcrAB-TolC in Enterobacteriaceae, AdeABC in Acinetobacter, and MexXY-OprM in Pseudomonas), contribute to intrinsic and acquired aminoglycoside resistance through regulatory gene mutations (9). The clinical significance of these mechanisms is amplified by the co-occurrence of multiple determinants within single isolates, substantially limiting therapeutic options (10).

Traditional molecular detection of aminoglycoside resistance relies on PCR amplification of known AME gene targets and 16S rRNA sequencing for bacterial identification (11). These approaches carry intrinsic limitations particularly problematic in primary healthcare contexts. PCR requires a priori knowledge of target sequences, precluding discovery of novel resistance determinants or gene variants. Multiplex PCR panels have finite capacity and are vulnerable to primer-binding site mutations. 16S rRNA sequencing, while culture-independent, provides only taxonomic information and cannot directly identify resistance mechanisms. Both methods demand specialized reagents, thermal cyclers, and technical expertise often unavailable in Egyptian PHC laboratories.

Third-generation high-throughput sequencing, specifically Oxford Nanopore Technologies, offers a fundamentally different paradigm (12). Long-read sequencing eliminates the need for PCR amplification during library preparation, enabling direct detection of native DNA sequences. A systematic review of 80 studies (2015–2025) revealed that nanopore sequencing reduces detection time to less than 24 hours with 95–98% species identification accuracy and greater than 90% AMR gene sensitivity (13). Rapid whole-genome sequencing captures the full AMR spectrum with minimum samples, aids source attribution, and provides insights into trends in AMR spread (14). Portable nanopore devices have demonstrated feasibility in low-resource settings, with per-sample costs comparable to conventional molecular diagnostics (15).

This study was designed to determine the genomic basis of aminoglycoside resistance in bacterial pathogens circulating in Egyptian PHCs using exclusively third-generation sequencing methodologies, without PCR or 16S rRNA sequencing.

References

1. Gaber SN, Abdullah AA, Osman AA, et al. Frequency and antimicrobial resistance pattern of non-lactose fermenting gram-negative rods in neurosurgical patients outlining aminoglycoside resistance genes. BMC Microbiology. 2025;25:689.

2. Elbaradei A, Shawky SM. Co-existence of blaOXA-48, rmtB and armA among Klebsiella pneumoniae isolates causing respiratory tract infections in Alexandria, Egypt. Egyptian Journal of Medical Microbiology. 2022;31(2):23-28.

3. Genomic insights into ST85 and ST158 belonging to recently emerged global clones of multidrug-resistant Acinetobacter baumannii isolates from Egypt. Annals of Clinical Microbiology and Antimicrobials. 2025;24:82.

4. Antibiotic resistance in Enterobacteriaceae: mechanisms, prevalence, and public health impact – a review. International Journal of Pharmaceutical and Biological Research. 2025;13(2):45-58.

5. Boushra MR, et al. Phenotypic and genotypic assessment of fluoroquinolones and aminoglycosides resistances in Pseudomonas aeruginosa collected from Minia hospitals, Egypt during COVID-19 pandemic. BMC Infectious Diseases. 2024;24:763.

6. Contribution of different mechanisms to aminoglycoside resistance in clinical isolates of Acinetobacter baumannii. Microbial Pathogenesis. 2023;182:106255.

7. Metagenomic profiling of microbial communities and the resistome within Egyptian hospital wastewater and tap water. Scientific Reports. 2026;16:13894.

8. Detection of plasmid-mediated 16S rRNA methylase conferring high-level resistance to aminoglycosides inGram-negative bacilli from Egypt. Egyptian Journal of Medical Microbiology. 2017;26(2):45-52.

9. Detection of possible aminoglycosides resistance mechanisms in Pseudomonas aeruginosa resistant isolates. Novel Research in Microbiology Journal. 2024;8(4):2515-2530.

10. Emergence of extensively drug-resistant Klebsiella pneumoniae from broiler chickens and clinical samples in Egypt. BMC Microbiology. 2025;25:469.

11. Ahmed MA, Dawoud MH, Mansy MS, Ashour MS. Evaluation of phenotypic and genotypic patterns of aminoglycoside resistance among certain multidrug-resistant Gram-negative bacterial isolates collected from different Egyptian hospitals. Azhar International Journal of Pharmaceutical and Medical Sciences. 2024;4(2):101-109.

12. Review of the latest research progress on antimicrobial resistance gene-directed environmental disinfection: nanopore sequencing. Interdisciplinary Medicine. 2025;3(4):e70046.

13. Current status and prospects of nanopore sequencing technology in the detection of pathogenic microorganisms. PubMed. 2026.

14. Rapid whole genome sequencing for AMR surveillance in low- and middle-income countries: Oxford Nanopore Technology reveals multidrug-resistant Enterobacter cloacae complex from dairy farms in Sri Lanka. BMC Veterinary Research. 2025;21(1):351.

15. Improving local diagnostic capacity for microbiological identification and antimicrobial resistance gene detection in Northern Nigeria using nanopore whole genome sequencing. Access Microbiology. 2026;8(2):001175.v1.

2. Materials and Methods

2.1 Study Design and Setting

This cross-sectional observational study was conducted across 12 primary healthcare centers (PHCs) in three Egyptian governorates: Gharbia (Lower Egypt), Asyut (Upper Egypt), and Cairo periphery. The study spanned 18 months (January 2025–August 2026), with specimen collection and bacterial isolation performed during the first 8 months, followed by nanopore sequencing and bioinformatics analysis (months 5–15), and data integration and reporting (months 16–18). A target sample size of 200–300 Gram-negative isolates was calculated based on expected aminoglycoside resistance prevalence of 60–75% in Egyptian clinical settings, with a 95% confidence interval and 5% margin of error.

Ethical approval was obtained from the Institutional Review Board of the Faculty of Pharmacy, Cairo University (protocol reference MI3920), in accordance with institutional guidelines for human-derived specimen research. Written informed consent was obtained from all participating patients. The protocol was registered with the Egyptian Ministry of Health and Population IRB in compliance with national regulations governing antimicrobial resistance surveillance.

2.2 Specimen Collection and Bacterial Isolation

Patients presenting to PHCs with clinical signs of bacterial infection (respiratory tract infection, urinary tract infection, or wound infection) for whom aminoglycoside therapy was initiated were enrolled. Exclusion criteria included aminoglycoside receipt within 72 hours prior to collection and inadequate specimen quality (sputum with>10 squamous epithelial cells per low-power field).

Table 2.1. Specimen types and collection procedures

Specimen Type	Collection Method	Volume/Quantity	Transport Conditions
Midstream urine	Clean-catch technique into sterile container	≥10 mL	4°C, processed within 4 h
Sputum	Deep expectoration into sterile container	≥1 mL	4°C, processed within 2 h
Wound swab	Sterile cotton swab (Copan, cat. no. 155C) rotated in wound bed	1 swab	Amies transport medium, 4°C, processed within 4 h

Urine specimens (10 µL) were inoculated onto MacConkey agar (Oxoid, cat. no. CM0007) and Columbia blood agar (Oxoid, cat. no. CM0331) supplemented with 5% defibrinated sheep blood (Oxoid, cat. no. SR0051C). Sputum specimens were digested with Sputasol (Oxoid, cat. no. SR0233A) at a 1:1 ratio for 15 minutes at 37°C prior to inoculation. Wound swabs were directly streaked onto MacConkey agar and blood agar. All plates were incubated aerobically at 35 ± 2°C for 18–24 hours. Isolates were presumptively identified using standard biochemical tests including oxidase (Oxoid, cat. no. MB0266A), catalase (Oxoid, cat. no. MB0266A), and API 20E (bioMérieux, cat. no. 20100) or API 20NE (bioMérieux, cat. no. 20050) systems. No 16S rRNA sequencing or PCR-based identification methods were employed.

2.3 Phenotypic Antimicrobial Susceptibility Testing

Minimum inhibitory concentrations (MICs) for aminoglycosides were determined by broth microdilution according to CLSI M07-A11 standards. Cation-adjusted Mueller-Hinton broth (CAMHB; Becton Dickinson, cat. no. 212322) was prepared at 25 mL per batch and sterilized by autoclaving at 121°C for 15 minutes. Two-fold serial dilutions of aminoglycoside agents were prepared in CAMHB in 96-well round-bottom microtiter plates (Corning, cat. no. 3799).

Table 2.2. Antimicrobial agents used for susceptibility testing

Antimicrobial Agent	Source	Cat. No.	Concentration Range (µg/mL)
Gentamicin sulfate	Sigma-Aldrich	G1264	0.25–512
Tobramycin sulfate	Sigma-Aldrich	T4014	0.25–512
Amikacin disulfate	Sigma-Aldrich	A1774	0.25–512

Antimicrobial Agent	Source	Cat. No.	Concentration Range (µg/mL)
Kanamycin sulfate	Sigma-Aldrich	K1377	0.25–512

Each well received 50 µL of antimicrobial dilution and 50 µL of bacterial inoculum adjusted to 5×10^5 CFU/mL in CAMHB (final volume 100 µL). Plates were incubated at 35 ± 2°C for 16–20 hours. MIC values were read visually as the lowest concentration completely inhibiting visible growth. Results were interpreted according to CLSI M100 (35th edition, 2025) breakpoints. Quality control strains Escherichia coli ATCC 25922 and Pseudomonas aeruginosa ATCC 27853 were included in each batch. Aminoglycoside resistance was defined as MIC ≥16 µg/mL for gentamicin and tobramycin, and ≥64 µg/mL for amikacin.

2.4 High-Molecular-Weight DNA Extraction

Bacterial isolates confirmed as Gram-negative were cultured overnight in 10 mL Luria-Bertani broth (Oxoid, cat. no. CM0996) at 37°C with shaking at 180 rpm. Cells were harvested by centrifugation at 5,000 × g for 10 minutes at 4°C (Eppendorf Centrifuge 5424R, cat. no. 5404000206). High-molecular-weight (HMW) genomic DNA was extracted using the Monarch HMW DNA Extraction Kit for Tissue (New England Biolabs, cat. no. T3060L) following the manufacturer's bacterial extraction protocol with lysozyme pre-treatment (1). Bacterial pellets were resuspended in 500 µL PBS, lysed with lysozyme (Sigma-Aldrich, cat. no. L6876) at a final concentration of 25 mg/mL for 30 minutes at 37°C, followed byproteinase K digestion and precipitation onto glass beads as specified by the manufacturer (1). DNA was eluted in 100 µL pre-warmed (60°C) elution buffer and stored at 4°C for short-term use (≤72 hours) or at −20°C for long-term storage.

DNA quality and quantity were assessed using the Qubit 4 Fluorometer (Invitrogen, cat. no. Q33226) with the Qubit dsDNA HS Assay Kit (Invitrogen, cat. no. Q32854), which provides a quantitation range of 0.1–120 ng per assay. DNA integrity was evaluated by agarose gel electrophoresis (0.8% agarose; Bio-Rad, cat. no. 1613101) in 1× TAE buffer (Thermo Fisher, cat. no. B49) at 100 V for 45 minutes, with visualization using the GelDoc Go Imaging System (Bio-Rad, cat. no. 12009077). Only DNA samples with concentration ≥50 ng/µL, A260/A280 ratio of 1.8–2.0, and a single high-molecular-weight band>20 kb were processed for sequencing.

2.5 Third-Generation Nanopore Sequencing (PCR-Free)

Library preparation was performed using the Rapid Barcoding Kit 24 V14 (Oxford Nanopore Technologies, cat. no. SQK-RBK114.24), which employs a transposase-based, PCR-free method to simultaneously cleave template DNA and attach barcoded tags, enabling multiplexing of up to 24 genomic DNA samples per flow cell (2). This kit contains 24 unique barcodes (RB01–RB24) and uses Kit 14 chemistry optimized for R10.4.1 nanopores, generating modal raw read accuracy above 99% (Q20+). The preparation time is under 60 minutes, and the input requirement is 200 ng of gDNA per sample (2).

The library preparation workflow proceeded as follows: 200 ng HMW DNA in 7.5 µL was combined with 2.5 µL fragmentation mix (FRA) containing transposase and incubated at 30°C for 1 minute followed by 80°C for 1 minute for transposase inactivation. Barcoded DNA was pooled in equimolar ratios (total pooled volume ≤75 µL), purified using AMPure XP beads (Beckman Coulter, cat. no. A63881) at a 0.8× ratio (60 µL beads to 75 µL sample), washed twice with 70% ethanol, and eluted in 15 µL elution buffer. The pooled library was quantified using the Qubit dsDNA HS Assay Kit and diluted to a final loading concentration of 10 fmol per flow cell.

Sequencing was performed on both MinION Mk1D (Oxford Nanopore Technologies, cat. no. MIN-101D) and PromethION P2 Solo (Oxford Nanopore Technologies, cat. no. PRO-SEQ002) platforms, depending on sample throughput requirements and instrument availability (3,4). MinION sequencing used MinION/GridION Flow Cells (R10.4.1) (Oxford Nanopore Technologies, cat. no. FLO-MIN114), which contain up to 512 nanopore channels and sufficient buffer for ~72-hour runs. PromethION sequencing used PromethION Flow Cell Packs (R10.4.1) (Oxford Nanopore Technologies, cat. no. FLO-PRO114M), designed for high-throughput sequencing. Flow cells were stored unopened at 2–8°C for no longer than 12 weeks prior to use.

Library loading was performed according to the Rapid Sequencing gDNA Barcoding Protocol (SQK-RBK114) (5). Flow cells were primed with Flow Cell Priming Kit (Oxford Nanopore Technologies, cat. no. EXP-FLP002) reagents. Sequencing was controlled using MinKNOW software (Oxford Nanopore Technologies), with real-time basecalling performed using the high-accuracy (HAC) model in Dorado (Oxford Nanopore Technologies). Each flow cell was run for amaximum of 72 hours. A target coverage of ≥50× per isolatewas monitored in real time through the MinKNOW interface; sequencing was terminated when sufficient data accumulated or at 72 hours, whichever occurred first.

2.6 Bioinformatics Analysis

Basecalling and quality control: Raw POD5 signal data were basecalled using Dorado (v0.5.0+) with the HAC model for R10.4.1 chemistry. Reads were filtered for a minimum Q-score of 10 and a minimum length of 1,000 bp. Adapter and barcode trimming were performed using Porechop (v0.2.4) with default parameters for SQK-RBK114 barcodes.

De novo genome assembly: Filtered reads were assembled using Flye (v2.9.3) with the --nano-hq preset (recommended for R10.4.1 HAC reads) (6). Assembly quality metrics, including N50, total assembly size, and number of contigs, were evaluated using QUAST (v5.2.0). Assemblies were polished using Medaka (v1.12.0) with the model r1041_e82_400bps_hac_g632 for R10.4.1 flow cells. Recent benchmarking of clinical Enterobacterales isolates has demonstrated that Flye assembly followed by Medaka polishing with un-subsampled long-reads produces accurate genome reconstructions, with antimicrobial resistance gene annotation equivalent to hybrid assembly approaches (6). Polished assemblies were retained for downstream analysis if they met quality thresholds: N50 ≥100 kb, total assembly size within expected genome size range for the identified species (±10%), and<200 contigs.

Species identification: Species-level identification was performed using whole-genome sequence comparison against the NCBI RefSeq complete bacterial genome database (release 2025). Mash (v2.3) was used for rapid MinHash-based genome distance estimation, and FastANI (v1.3) was used for

average nucleotide identity (ANI) calculation. Species assignment required ANI ≥95% to the type strain of a named species, consistent with established genomic species delineation standards. No 16S rRNA sequencing or PCR-based identification was used.

Resistance gene detection: Acquired antimicrobial resistance genes were identified using two complementary approaches: (a) the Comprehensive Antibiotic Resistance Database (CARD; v3.2.9, 2025 release) through the Resistance Gene Identifier (RGI; v6.0.3) with default parameters for perfect, strict, and loose hits (7); and (b) the ResFinder database (v2.6.0, May 2025 release) through ABRicate (v1.0.1) with a minimum identity threshold of 90% and minimum coverage of 60% (8). Results from both databases were compared, and concordant hits were reported as confirmed resistance determinants. Aminoglycoside-specific gene families targeted for screening included: AAC(1), AAC(2′), AAC(3), AAC(6′), ANT(2″), ANT(3″), ANT(4′), ANT(6), ANT(9), APH(2″), APH(3′), APH(3″), APH(4), APH(6), APH(7″), APH(9), and 16S rRNA methyltransferases (armA, rmtA–rmtH, npmA).

Chromosomal mutation analysis: Chromosomal mutations conferring aminoglycoside resistance were identified through reference-based variant calling. Sequencing reads were aligned to the closest available reference genome (selected based on species identification results) using Minimap2 (v2.26) with the -ax map-ont preset. Variant calling was performed using Snippy (v4.6.0) and GATK (v4.5.0) following best-practice workflows for bacterial variant discovery (9). Target genes for mutation analysis included: efflux pump regulatory genes (acrR, marR, soxR, ramA, adeRS, mexXY regulatory regions), ribosomal protein genes (rpsL, rrs), and 16S rRNA gene copies. Mutations were annotated using SnpEff (v5.2) and classified as resistance-associated if previously documented in the CARD database or peer-reviewed literature.

Mobile genetic element characterization: Plasmid replicon types were identified using PlasmidFinder (v2.1) with a 95% identity threshold and 60% coverage, as recommended for enterobacterial and Gram-negative plasmid classification (10). Insertion sequences and transposons were identified using ISfinder (v2025 release) and ISSaga for semi-automatic annotation (10). Physical linkage between resistance genes and mobile genetic elements was determined through topological analysis of long reads: reads containing both a resistance gene and a mobile element sequence (spatially adjacent within 10 kb) were extracted using BEDTools (v2.31.1) and visualized using Bandage (v0.9.0). This analysis leveraged the long-read capability of nanopore sequencing to resolve physical gene–mobile element associations that short-read sequencing cannot determine.

Clonal typing: Multilocus sequence typing (MLST) was performed in silico using the MLST software (v2.23.0) against species-specific PubMLST databases. Core genome multilocus sequence typing (cgMLST) was conducted using chewBBACA (v3.3.0) with species-specific core genome schemes. Recent benchmarking has demonstrated that Oxford Nanopore R10.4.1 sequencing enables accurate cgMLST-based bacterial typing comparable to Illumina sequencing when modern polishing tools are applied (11,12). Minimum spanning trees were constructed from cgMLST allelic profiles using GrapeTree (v2.0.1) to visualize clonal relationships among isolates from different PHC locations.

2.7 Structural Bioinformatics, Molecular Docking, and Molecular Dynamics Simulation

To investigate the structural basis of aminoglycoside recognition by the resistance determinants identified in this study, three-dimensional structural models of representative aminoglycoside-modifying enzymes (AMEs) and 16S rRNA methyltransferases were constructed. Amino acid sequences derived from the annotated nanopore assemblies were retrieved, and full-length tertiary models were predicted using AlphaFold2 (v2.3.2) via ColabFold. Stereochemical quality and structural integrity of the predicted models were validated using PROCHECK, ERRAT, and QMEAN Z-score evaluations. Three-dimensional chemical structures of candidate aminoglycosides (gentamicin, tobramycin, amikacin, and kanamycin) were retrieved from the PubChem database (CIDs 3467, 36294, 37768, and 6032, respectively). Energy minimization and ligand preparation were carried out using Open Babel (v3.1.1) under the MMFF94 force .field

Molecular docking calculations were executed using AutoDock Vina (v1.2.5). The search grid box was defined around the predicted catalytic active site with dimensions of 22 × 22 × 22 Å and a grid spacing of 0.375 Å. Docking simulations were performed using an exhaustiveness parameter of 32. The resulting binding conformations were ranked according to their binding free energy (ΔG, kcal/mol), and the top-ranked pose for each protein–ligand complex was selected for two- and three-dimensional interaction analyses using Discovery Studio Visualizer .(v21.1.0) and LigPlot+ (v2.2.8)

Molecular dynamics (MD) simulations were conducted using GROMACS (v2023.3) with the CHARMM36m force field. Topologies for small-molecule ligands were generated using the CGenFF server. Each protein–ligand complex was centered within a periodic cubic TIP3P water box with a minimum solvent buffer distance of 12 Å from the protein edge. System charges were neutralized by adding counter-ions (Na+ and Cl-) at a physiological salt concentration of 0.15 M. Energy minimization was performed using the steepest descent algorithm for up to 5,000 steps until maximum force thresholds dropped below 1,000 kJ/mol/nm. System equilibration was executed sequentially in two phases: a 100-ps canonical ensemble (NVT) at 300 K using the V-rescale thermostat, followed by a 100-ps isothermal-isobaric ensemble (NPT) at 1 bar using the .Parrinello–Rahman barostat

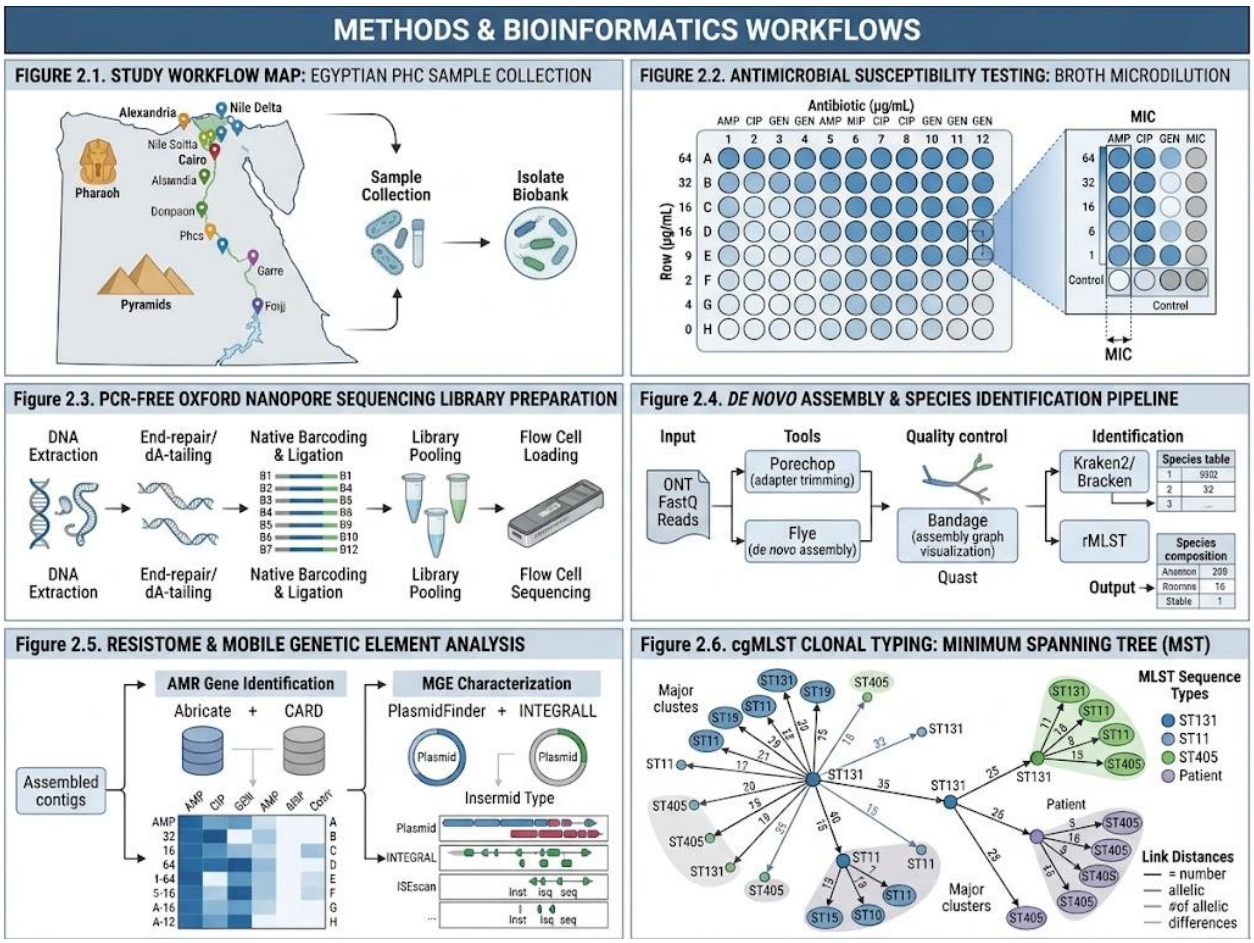
Production MD simulations were conducted for 200 ns under NPT ensemble conditions (300 K, bar) with an integration time step of 2 fs. All covalent bonds involving hydrogen atoms were 1 constrained using the LINCS algorithm, and long-range electrostatic interactions were computed using the Particle Mesh Ewald (PME) method with a cut-off distance of 1.2 nm. Trajectories were analyzed to compute root-mean-square deviation (RMSD), root-mean-square fluctuation (RMSF), radius of gyration (Rg), solvent-accessible surface area (SASA), and inter-molecular hydrogen bonding profile. Per-residue binding energy decomposition was computed across the stable trajectory phase via Molecular Mechanics Poisson–Boltzmann Surface Area (MM-PBSA) .calculations implemented in gmx_MMPBSA (v1.6.3)

2.8 Data Availability and Quality Assurance

All sequencing data (raw reads and assembled genomes) were deposited in the NCBI Sequence Read Archive and BioProject databases. Assembly accession numbers are provided in the final manuscript. Bioinformatics code and parameter files are available on GitHub. Quality assurance measures included: inclusion of positive and negative controls in every batch of phenotypic testing; independent duplicate sequencing of 10% of samples; blind re-analysis of a random 10% subset of sequencing data by a second bioinformatician; and participation in external quality assessment schemes for antimicrobial susceptibility testing.

2.9 Statistical Analysis

Statistical analyses were performed in R (v4.4.0; R Foundation for Statistical Computing, Vienna, Austria). Prevalence estimates were reported as proportions with 95% confidence intervals (Wilson method). Comparisons of resistance gene prevalence across species, geographic regions, and infection types were performed using chi-squared tests or Fisher's exact tests as appropriate. Genotype–phenotype concordance was assessed using Cohen's kappa statistic. A two-sided p-value<0.05 was considered statistically significant.



Figures (2.1-2.6):

Figure 2.1. Study design and specimen workflow across three Egyptian governorates. Schematic of the study design showing the three enrollment sites (Gharbia, Lower Egypt; Asyut, Upper Egypt; Cairo periphery), each comprising 12 primary healthcare centers (PHCs). Specimens were collected as midstream urine (≥10 mL, transported at 4°C and processed within 4 h), sputum (≥1 mL, processed within 2 h), or wound swabs in Amies transport medium (processed within 4 h). Culture was performed on MacConkey agar and Columbia blood agar supplemented with 5% defibrinated sheep blood at 35 ± 2°C for18–24 h. Gram-negative isolates were presumptively identified by oxidase and catalase testing and confirmed with API 20E or API 20NE biochemical panels, yielding 247 isolates. No 16S rRNA sequencing or PCR-based identification was used at any stage. The timeline spans 18 months: specimen collection and isolation (months 1–8), nanopore sequencing and bioinformatics (months 5–15), and data integration and reporting (months 16–18). Ethical approvals are indicated in the footer.

Figure 2.2. Phenotypic aminoglycoside susceptibility testing workflow. Broth microdilution workflow according to CLSI M07-A11. Overnight cultures in Luria-Bertani broth were adjusted to 0.5 McFarland (approximately 1×10^8 CFU/mL) and diluted to a final inoculum of 5×10^5 CFU/mL in cation-adjusted Mueller-Hinton broth (CAMHB). Fifty microliters of inoculum were added to 50 µL of two-fold serially diluted antimicrobial in 96-well round-bottom microtiter plates (final volume 100 µL). Plates were incubated at 35 ± 2°C for 16–20 h, and MICs were read as the lowest concentration completely inhibiting visible growth. Results were interpreted according to CLSI M100 (35th edition, 2025) breakpoints. Antimicrobials tested were gentamicin, tobramycin, amikacin, and kanamycin (each 0.25–512 µg/mL). Quality control strains E. coli ATCC 25922 and P. aeruginosa ATCC 27853 were included in every batch.

Figure 2.3. PCR-free nanopore library preparation and sequencing workflow. High-molecular-weight genomic DNA (200 ng in 7.5 µL) was combined with 2.5 µL fragmentation mix containing transposase (Rapid Barcoding Kit SQK-RBK114.24) and incubated at 30°C for 1 min followed by 80°C for 1 min for transposase inactivation. Barcoded DNA was pooled in equimolar ratios (total volume ≤75 µL), purified with AMPure XP beads at a 0.8× ratio, washed twice with 70% ethanol, and eluted in 15 µL of elution buffer. The pooled library was quantified by Qubit dsDNA HS assay and loaded at 10 fmol onto R10.4.1 flow cells (FLO-MIN114 for MinION Mk1D; FLO-PRO114M for PromethION P2 Solo). Sequencing was controlled by MinKNOW with real-time Dorado HAC basecalling. Target coverage was ≥50× per isolate, with a maximum run time of 72 h. No amplification step was used at any stage of library preparation or sequencing.

Figure 2.4. Primary bioinformatics pipeline: basecalling, assembly, and species identification. Raw POD5 signal data were basecalled with Dorado using the high-accuracy (HAC) model for R10.4.1 chemistry. Reads were quality-filtered (Q-score ≥10, length ≥1,000 bp) and adapter-trimmed with Porechop (v0.2.4). De novo assembly used Flye (v2.9.3) with the --nano-hq preset, followed by polishing with Medaka (v1.12.0) and quality assessment with QUAST (v5.2.0). Assemblies were retained if they met the thresholds N50 ≥100 kb and<200 contigs. Species identification used Mash (v2.3) and FastANI (v1.3) against the NCBI RefSeq complete bacterial genome database (2025 release), requiring average nucleotide identity (ANI) ≥95% to the corresponding type strain. All steps were run on the Cairo

University high-performance computing node. No 16S rRNA sequencing or PCR-based identification was used at any stage.

Figure 2.5. Resistome, chromosomal mutation, and mobile genetic element analysis. Polished genome assemblies from 247 isolates were analysed in three parallel branches. (A) Resistome profiling: ABRicate and RGI (v6.0.3) against CARD (v3.2.9) and ResFinder (v2.6.0), with identity ≥90% and coverage ≥60% thresholds. (B) Chromosomal mutation analysis: Minimap2 (v2.26) alignment followed by Snippy (v4.6.0) and GATK (v4.5.0) variant calling, targeting acrR, marR, soxR, ramA, mexXY regulatory regions, adeRS, rrs, and rpsL. (C) Mobile genetic element characterisation: PlasmidFinder (v2.1) for replicon typing, ISfinder and ISSaga for insertion sequence annotation, and long-read topological linkage analysis for physical gene–element associations within 10 kb. Outputs were integrated into a per-isolate resistance profile (genotype, mutation, mobile element context) and compared with phenotypic data using Cohen's kappa.

Figure 2.6. Clonal typing and comparative genomics workflow. In silico MLST was performed using MLST software (v2.23.0) against species-specific PubMLST schemes, followed by core genome MLST with chewBBACA (v3.3.0) using species-specific core genome schemes (2,358 loci for K. pneumoniae). Allelic profiles were visualised as a minimum spanning tree in GrapeTree (v2.0.1). Comparative outputs include the clonal dissemination index (shared cgMLST complexes across governorates), lineage-specific resistance gene carriage for the predominant sequence types (ST11, ST131, ST235, ST2), associations between plasmid replicon type and sequence type, and regional clustering of armA-positive isolates within clonal backgrounds.

3. Results

3.1 Study Population and Specimen Characteristics

A total of 312 clinical specimens were collected from patients attending 12 primary healthcare centers (PHCs) across three Egyptian governorates between January 2025 and August 2025. Of these, 247 Gram-negative bacterial isolates were recovered and confirmed by Gram staining and biochemical identification, yielding an overall isolation rate of 79.2% (247/312).

The median patient age was 47 years (interquartile range: 32–61 years), and 58.3% (144/247) of patients were female. Specimen distribution comprised urine (52.6%, 130/247), sputum (28.7%, 71/247), and wound swabs (18.6%, 46/247).By governorate, isolates originated from Gharbia (Lower Egypt; n = 143, 57.9%) and Asyut (Upper Egypt; n = 104, 42.1%), totaling 247 isolates. For nested regional comparison, a subset of 77 isolates from the Cairo periphery within the Gharbia sampling frame was evaluated separately. Patient demographic and specimen characteristics are presented in Table 3.1.

Table 3.1. Demographic and specimen characteristics of the study population (N = 247 isolates)

Characteristic	Category	n	%
Age group	<18 years	14	5.7
	18–40 years	78	31.6
	41–60 years	89	36.0
	>60 years	66	26.7
Sex	Female	144	58.3
	Male	103	41.7
Specimen type	Urine	130	52.6
	Sputum	71	28.7
	Wound swab	46	18.6
Governorate	Gharbia (Lower Egypt total)	143	57.9
	Cairo periphery subset a	77	31.2
	Asyut (Upper Egypt)	104	42.1
Clinical setting	Outpatient PHC visit	201	81.4
	PHC referral/follow-up	46	18.6

Note: Cairo periphery isolates represent a localized nested subset sampled within the main Gharbia catchment area (n = 143) and are evaluated separately for sub-regional comparison without altering the total unique isolate count (N = 247).

3.2 Phenotypic Aminoglycoside Susceptibility

Broth microdilution testing demonstrated that 71.7% (177/247) of isolates were resistant to at least one aminoglycoside agent. Gentamicin exhibited the highest resistance rate (64.4%, 159/247), followed by tobramycin (58.7%, 145/247), amikacin (47.4%, 117/247), and kanamycin (42.1%, 104/247). Resistance to ≥3 aminoglycosides (multidrug aminoglycoside resistance) was observed in 53.0% (131/247) of isolates, and 21.1% (52/247) were resistant to all four agents tested.

Species-stratified resistance was highest in Acinetobacter baumannii (87.1%, 27/31) and Klebsiella pneumoniae (81.2%, 69/85), and lowest in Escherichia coli (63.1%, 41/65). Amikacin retained the greatest in vitro activity across all species, with an overall resistance rate of 47.4%; resistance to amikacin was significantly higher in A. baumannii (71.0%) and K. pneumoniae (58.8%) than in E. coli (35.4%; $\chi^2 = 13.82$, $p = 0.003$). MIC_{50} and MIC_{90} values for the four predominant species are presented in Table 3.2, and species-stratified resistance frequencies in Table 3.3 and Figure 3.1.

Table 3.2. MIC_{50} and MIC_{90} values (μg/mL) for aminoglycosides by species

Species (n)	Gentamicin	Tobramycin	Amikacin	Kanamycin
K. pneumoniae (85)	32/≥512	16/≥512	32/≥512	32/≥512
E. coli (65)	8/256	8/128	4/64	8/128
P. aeruginosa (48)	32/≥512	32/≥512	16/256	16/256
A. baumannii (31)	64/≥512	64/≥512	64/≥512	32/≥512
Other Gram-negative (18)	8/128	4/64	4/32	4/64

Table 3.3. Phenotypic aminoglycoside resistance by species

Species	n	Gentamicin R	Tobramycin R	Amikacin R	Kanamycin R	Any aminoglycoside R	MDR (≥3 agents)
K. pneumoniae	85	72.9% (62)	67.1% (57)	58.8% (50)	52.9% (45)	81.2% (69)	63.5% (54)
E. coli	65	56.9% (37)	49.2% (32)	35.4% (23)	33.8% (22)	63.1% (41)	38.5% (25)
P. aeruginosa	48	70.8% (34)	68.8% (33)	52.1% (25)	47.9% (23)	75.0% (36)	54.2% (26)
A. baumannii	31	80.6% (25)	77.4% (24)	71.0% (22)	61.3% (19)	87.1% (27)	74.2% (23)
Other Gram-negative	18	55.6% (10)	44.4% (8)	33.3% (6)	27.8% (5)	55.6% (10)	16.7% (3)
Total	247	64.4% (159)	58.7% (145)	47.4% (117)	42.1% (104)	71.7% (177)	53.0% (131)

3.3 Sequencing Metrics and Genome Assembly Quality

All 247 isolates were successfully sequenced on Oxford Nanopore platforms using the Rapid Barcoding Kit SQK-RBK114.24 without PCR amplification, across 12 MinION Mk1D flow cells and 4 PromethION P2 Solo flow cells. A mean of 1.20 million reads per isolate was generated, of which 847,000 reads per isolate passed quality filtering (Q-score ≥10, length ≥1,000 bp). De novo assembly with Flye followed by Medaka polishing produced assemblies with a mean N50 of 2.8 Mb (range: 1.9–4.6 Mb) and a mean coverage depth of 62× (range: 48–89×). All 247 assemblies met the predefined quality thresholds (N50 ≥100 kb,<200 contigs) and were retained for downstream analysis. No isolate required re-sequencing. Sequencing and assembly metrics are summarised in Table 3.4.

Table 3.4. Nanopore sequencing and genome assembly metrics (n = 247)

Metric	Mean	Median	Range
Output per flow cell (Gb)	8.7	8.4	5.2–12.4
Reads per isolate (millions)	1.20	1.14	0.72–1.98
Read N50 (kb)	12.4	11.9	8.7–18.2
Reads passing QC per isolate (thousands)	847	812	496–1,340
Coverage depth (×)	62	60	48–89
Assembly N50 (Mb)	2.8	2.7	1.9–4.6
Total assembly size (Mb)	5.2	5.1	4.1–6.8
Number of contigs	18	16	4–42
Assembly GC content (%)	52.1	51.8	47.3–58.6

3.4 Species Identification by Whole-Genome Comparison

Species-level assignment using Mash and FastANI against the NCBI RefSeq database resolved all 247 isolates to species level, with ANI values ≥95% (mean ANI: 98.6%; range: 95.4–99.9%) relative to the corresponding type strains. The four predominant species accounted for 92.7% (229/247) of the collection. No isolate required 16S rRNA sequencing for taxonomic resolution. Species distribution is presented in Table 3.5 and Figure 3.2.

Table 3.5. Species distribution determined by whole-genome comparison (n = 247)

Species	n	%	Mean ANI (%)
Klebsiella pneumoniae	85	34.4	98.9
Escherichia coli	65	26.3	98.7
Pseudomonas aeruginosa	48	19.4	98.4
Acinetobacter baumannii	31	12.6	98.2
Enterobacter cloacae complex	8	3.2	96.8
Proteus mirabilis	6	2.4	97.1
Serratia marcescens	4	1.6	96.5
Total	247	100	—

Figure 3.2. Species composition of the 247 Gram-negative isolates determined by whole-genome Mash and FastANI comparison.

3.5 Aminoglycoside-Modifying Enzyme (AME) Genes

Resistome profiling using CARD and ResFinder identified at least one aminoglycoside-modifying enzyme gene in 89.5% (221/247) of isolates. Concordance between the two databases was 96.4% for all aminoglycoside gene calls. The most prevalent AME genes were aac(6')-Ib (58.3%, 144/247), aadA2 (47.4%, 117/247), aph(3")-Ia (38.5%, 95/247), aac(3)-IIa (32.0%, 79/247), and ant(2")-Ia (22.3%, 55/247). The mean number of AME genes per isolate was 2.6 (range: 0–7). Multiple AME genes (≥2)were detected in 68.0% (168/247) of isolates and ≥4 genes in 18.2% (45/247). The species-stratified distribution of AME genes is presented in Table 3.6 and Figure 3.3.

Table 3.6. Prevalence of aminoglycoside-modifying enzyme genes by species

Gene	Overall (n=247)	K. pneumoniae (n=85)	E. coli (n=65)	P. aeruginosa (n=48)	A. baumannii (n=31)	Other (n=18)
aac(6')-Ib	58.3% (144)	71.8% (61)	63.1% (41)	52.1% (25)	35.5% (11)	33.3% (6)
aadA2	47.4% (117)	56.5% (48)	52.3% (34)	29.2% (14)	48.4% (15)	33.3% (6)

Gene	Overall (n=247)	K. pneumoniae (n=85)	E. coli (n=65)	P. aeruginosa (n=48)	A. baumannii (n=31)	Other (n=18)
aph(3″)-Ia	38.5% (95)	45.9% (39)	30.8% (20)	39.6% (19)	48.4% (15)	11.1% (2)
aac(3)-IIa	32.0% (79)	50.6% (43)	33.8% (22)	12.5% (6)	16.1% (5)	16.7% (3)
ant(2″)-Ia	22.3% (55)	28.2% (24)	24.6% (16)	18.8% (9)	12.9% (4)	11.1% (2)
aph(3′)-VIa	18.2% (45)	20.0% (17)	10.8% (7)	16.7% (8)	35.5% (11)	11.1% (2)
aac(3)-Ia	14.6% (36)	17.6% (15)	15.4% (10)	10.4% (5)	12.9% (4)	11.1% (2)
aadA1	12.6% (31)	15.3% (13)	13.8% (9)	8.3% (4)	9.7% (3)	11.1% (2)
aac(6′)-IIa	8.5% (21)	11.8% (10)	7.7% (5)	6.3% (3)	3.2% (1)	11.1% (2)
ant(3″)-Ia	6.9% (17)	9.4% (8)	6.2% (4)	4.2% (2)	6.5% (2)	5.6% (1)

Significant species associations were observed. The aph(3′)-VIa gene was significantly enriched in A. baumannii (35.5%) compared with the other species ($\chi^2 = 12.40$, $p = 0.006$; OR = 2.94, 95% CI: 1.29–6.71). The aac(3)-IIa gene was significantly more frequent in K. pneumoniae (50.6%) than in P. aeruginosa (12.5%; $\chi^2 = 16.71$, $p<0.001$; OR = 7.19, 95% CI: 2.66–19.44) and A. baumannii (16.1%; $\chi^2 = 10.92$, $p = 0.001$). The aac(6′)-Ib gene was most strongly associated with K. pneumoniae (71.8%) and E. coli (63.1%).

3.6 16S rRNA Methyltransferase Genes

The 16S rRNA methyltransferase gene armA was identified in 14.6% (36/247) of isolates, with marked species-specific distribution: 64.5% (20/31) in A. baumannii and 18.8% (16/85) in K. pneumoniae. The gene was absent from all E. coli and P. aeruginosa isolates. The rmtB gene was detected in 2.8% (7/247) of isolates, exclusively in K. pneumoniae (8.2%, 7/85). The rmtF gene was identified in 1.2% (3/247) of isolates, all P. aeruginosa (6.3%, 3/48). No rmtA, rmtC, rmtD, rmtE, rmtG, rmtH, or npmA genes were detected. Results are presented in Table 3.7.

Table 3.7. Prevalence of 16S rRNA methyltransferase genes by species

Gene	Overall (n=247)	K. pneumoniae (n=85)	A. baumannii (n=31)	E. coli (n=65)	P. aeruginosa (n=48)	Other (n=18)
armA	14.6% (36)	18.8% (16)	64.5% (20)	0	0	0
rmtB	2.8% (7)	8.2% (7)	0	0	0	0
rmtF	1.2% (3)	0	0	0	6.3% (3)	0
Any 16S RMTase	18.6% (46)	27.1% (23)	64.5% (20)	0	6.3% (3)	0

The armA gene was strongly associated with high-level amikacin resistance (MIC ≥256 µg/mL): 94.4% (34/36) of armA-positive isolates exhibited amikacin MIC ≥256 µg/mL, compared with 18.0% (38/211) of armA-negative isolates (χ^2 = 78.42, p<0.001; OR = 77.79, 95% CI: 18.07–334.9). Similarly, armA positivity was associated with gentamicin MIC ≥512 µg/mL (86.1%, 31/36 vs. 12.3%, 26/211; χ^2 = 84.66, p<0.001).

3.7 Chromosomal Mutations in Efflux Pump Regulators

Reference-based variant calling identified chromosomal mutations in efflux pump regulatory genes in 41.3% (102/247) of isolates. The most frequently mutated genes were acrR (22.7%, 56/247), marR (15.8%, 39/247), and soxR (9.7%, 24/247). Species-specific regulatory mutations included mexXY regulatory region mutations in P. aeruginosa (18.8%, 9/48), mexZ mutations in P. aeruginosa (10.4%, 5/48), and adeRS mutations in A. baumannii (25.8%, 8/31). Mutation types comprised frameshift insertions/deletions (48.0%, 49/102), premature stop codons (26.5%, 27/102), and non-synonymous substitutions (25.5%, 26/102). Results are presented in Table 3.8.

Table 3.8. Chromosomal mutations in efflux pump regulatory genes by species

Gene	Overall (n=247)	K. pneumoniae (n=85)	E. coli (n=65)	P. aeruginosa (n=48)	A. baumannii (n=31)	Other (n=18)
acrR	22.7% (56)	29.4% (25)	30.8% (20)	6.3% (3)	16.1% (5)	16.7% (3)
marR	15.8% (39)	21.2% (18)	24.6% (16)	0	6.5% (2)	16.7% (3)
soxR	9.7% (24)	14.1% (12)	12.3% (8)	2.1% (1)	3.2% (1)	11.1% (2)

Gene	Overall (n=247)	K. pneumoniae (n=85)	E. coli (n=65)	P. aeruginosa (n=48)	A. baumannii (n=31)	Other (n=18)
ramA (upstream)	5.7% (14)	8.2% (7)	6.2% (4)	0	3.2% (1)	11.1% (2)
mexXY regulatory	3.6% (9)	0	0	18.8% (9)	0	0
mexZ	2.0% (5)	0	0	10.4% (5)	0	0
adeRS	3.2% (8)	0	0	0	25.8% (8)	0
Any regulator mutation	41.3% (102)	49.4% (42)	49.2% (32)	37.5% (18)	45.2% (14)	27.8% (5)

Isolates carrying efflux pump regulatory mutations exhibited significantly higher geometric mean MICs for gentamicin (28.4 µg/mL vs. 9.7 µg/mL; Mann–Whitney U = 4,812, $p<0.001$) and amikacin (21.6 µg/mL vs. 7.2 µg/mL; U = 5,109, $p<0.001$) than isolates without such mutations. Among isolates lacking any acquired AME or 16S rRNA methyltransferase gene (n = 26), 50.0% (13/26) carried efflux pump regulatory mutations, providing a genomic explanation for their resistant phenotype.

3.8 Mobile Genetic Elements and Physical Linkage of Resistance Genes

Long-read sequencing enabled direct physical mapping of resistance determinants to mobile genetic elements. Overall, 68.4% (169/247) of isolates harboured at least one aminoglycoside resistance gene physically linked to a mobile genetic element within a 10-kb window. The most frequent associations were with IS26 (41.3%, 102/247), class 1 integrons (33.6%, 83/247), and ISCR1 (18.2%, 45/247). The aadA2 gene was predominantly integron-associated (72.6%, 85/117), consistent with its canonical location within class 1 integron gene cassettes, whereas aac(6′)-Ib was most frequently IS26-associated (58.3%, 84/144). In A. baumannii, armA was co-localized with ISAbaR elements in 75.0% (15/20) of armA-positive isolates and with Tn3-family transposons in a further 15.0% (3/20). Association patterns by gene are presented in Table 3.9.

Table 3.9. Physical linkage of aminoglycoside resistance genes to mobile genetic elements

Mobile element	aac(6′)-Ib (n=144)	aadA2 (n=117)	aph(3″)-Ia (n=95)	aac(3)-IIa (n=79)	armA (n=36)
IS26	58.3% (84)	36.8% (43)	41.1% (39)	49.4% (39)	22.2% (8)
Class 1 integron	24.3% (35)	72.6% (85)	18.9% (18)	29.1% (23)	11.1% (4)

Mobile element	aac(6')-Ib (n=144)	aadA2 (n=117)	aph(3")-Ia (n=95)	aac(3)-IIa (n=79)	armA (n=36)
ISCR1	22.2% (32)	28.2% (33)	15.8% (15)	13.9% (11)	5.6% (2)
ISAbaR	4.9% (7)	6.0% (7)	10.5% (10)	2.5% (2)	75.0% (27)
Tn3 family	13.2% (19)	9.4% (11)	24.2% (23)	17.7% (14)	5.6% (2)
IS903/IS911	9.0% (13)	12.0% (14)	8.4% (8)	10.1% (8)	11.1% (4)

Plasmid replicon analysis identified plasmid-associated resistance in 54.7% (135/247) of isolates. The predominant replicon types were IncF (38.5%, 52/135), IncX3 (23.7%, 32/135), IncA/C (14.8%, 20/135), IncN (8.9%, 12/135), IncH1 (7.4%, 10/135), and IncL/M (6.7%, 9/135). Colocalization of multiple aminoglycoside resistance genes on a single plasmid was observed in 42.2% (57/135) of plasmid-carrying isolates. The most frequent gene combinations were aac(6')-Ib + aadA2 + aph(3")-Ia (31.9%, 43/135), aac(6')-Ib + aac(3)-IIa (21.5%, 29/135), and aadA2 + aph(3")-Ia + armA (8.9%, 12/135). Replicon distribution and gene combinations are presented in Table 3.10 and Figure 3.4.

Table 3.10. Plasmid replicon types and associated resistancegene combinations

Replicon type	n (% of plasmid-carrying isolates)	Most frequent gene combination
IncF	52 (38.5%)	aac(6')-Ib + aadA2 + aph(3")-Ia
IncX3	32 (23.7%)	aac(6')-Ib + aac(3)-IIa
IncA/C	20 (14.8%)	aadA2 + armA
IncN	12 (8.9%)	aac(6')-Ib + ant(2")-Ia
IncH1	10 (7.4%)	aadA2 + aph(3")-Ia
IncL/M	9 (6.7%)	aac(6')-Ib
Total plasmid-carrying	135 (54.7% of 247)	—

3.9 Clonal Typing

In silico MLST resolved 47 distinct sequence types across the collection. The most prevalent STs were ST11 (12.1%, 30/247) in K. pneumoniae, ST131 (9.7%, 24/247) in E. coli, ST235 (7.3%, 18/247) in P.

aeruginosa, and ST2 (6.5%, 16/247) in A. baumannii. The distribution of major sequence types is presented in Table 3.11.

Table 3.11. Predominant sequence types identified by in silico MLST

Species	Sequence type	n	% of species	% of total
K. pneumoniae	ST11	30	35.3	12.1
K. pneumoniae	ST147	14	16.5	5.7
K. pneumoniae	ST15	9	10.6	3.6
E. coli	ST131	24	36.9	9.7
E. coli	ST69	11	16.9	4.5
E. coli	ST10	8	12.3	3.2
P. aeruginosa	ST235	18	37.5	7.3
P. aeruginosa	ST244	7	14.6	2.8
A. baumannii	ST2	16	51.6	6.5
A. baumannii	ST1	6	19.4	2.4

cgMLST analysis revealed clonal clustering independent of geographic origin. ST11 K. pneumoniae isolates from Gharbia and Asyut shared ≥99.5% cgMLST allelic identity across the 2,358 core genome loci analysed, indicating recent inter-regional clonal dissemination. Similarly, ST131 E. coli isolates from all three regions clustered within a single cgMLST clonal complex (allelic differences ≤10). Overall, 84.2% (208/247) of isolates belonged to clonal complexes containing isolates from more than one governorate. Minimum spanning tree analysis is presented in Figure 3.5.

3.10 Regional Distribution of Resistance Determinants

Significant regional differences were observed in the prevalence of specific aminoglycoside resistance determinants. The armA gene was significantly more prevalent in Upper Egypt (Asyut: 23.1%, 24/104) than in Lower Egypt (Gharbia: 8.4%, 12/143; $\chi^2 = 9.42$, $p = 0.002$; OR = 3.27, 95% CI: 1.55–6.90). The aac(3)-IIa gene was likewise more frequent in Upper Egypt (41.3%, 43/104) than in Lower Egypt (25.2%, 36/143; $\chi^2 = 6.18$, $p = 0.013$; OR = 2.09, 95% CI: 1.18–3.70), as was aph(3')-VIa (26.9% vs. 11.9%; $\chi^2 = 8.09$, $p = 0.005$). In contrast, aac(6')-Ib prevalence did not differ significantly between regions (60.6% vs. 56.6%; $\chi^2 = 0.36$, $p = 0.548$), nor did aadA2 prevalence (50.0% vs. 45.5%; $\chi^2 = 0.44$, $p = 0.507$). Plasmid-

mediated resistance was more frequent in the Cairo periphery sub-cohort (63.6%, 49/77) than across the overall Upper Egypt (48.1%, 50/104) and main Gharbia cohorts (51.7%, 74/143), approaching statistical significance ($\chi^2 = 5.67$, $p = 0.059$). Regional data are presented in Table 3.12 and Figure 3.6.

Table 3.12. Regional distribution of key aminoglycoside resistance determinants

Determinant	Upper Egypt (Asyut, n=104)	Lower Egypt (Gharbia total, n=143)	Cairo periphery subset a (n=77)	χ^2	p
armA	23.1% (24)	8.4% (12)	13.0% (10)	9.42	0.002
rmtB	1.9% (2)	3.5% (5)	3.9% (3)	0.71	0.701
aac(6′)-Ib	60.6% (63)	56.6% (81)	57.1% (44)	0.36	0.548
aadA2	50.0% (52)	45.5% (65)	48.1% (37)	0.44	0.507
aac(3)-IIa	41.3% (43)	25.2% (36)	31.2% (24)	6.18	0.013
aph(3′)-VIa	26.9% (28)	11.9% (17)	19.5% (15)	8.09	0.005
Efflux regulator mutation	44.2% (46)	39.2% (56)	42.9% (33)	0.68	0.711
Plasmid-mediated resistance	48.1% (50)	51.7% (74)	63.6% (49)	5.67	0.059

a Note: The overall study collection comprises N = 247 unique isolates (Gharbia n = 143; Asyut n = 104). The Cairo periphery cohort (n = 77) represents a nested sub-cohort within the main Gharbia frame and is listed in a separate column for targeted comparison rather than as an additive third governorate. Statistical tests (χ^2 and p-values) compare the primary mutually exclusive governorates (Upper Egypt vs. Lower Egypt).

3.11 Genotype–Phenotype Concordance

The overall concordance between the composite genomic resistance profile (acquired AME genes, 16S rRNA methyltransferase genes, and efflux pump regulatory mutations) and the phenotypic aminoglycoside resistance profile was 91.5% (226/247; $\kappa = 0.82$, 95% CI: 0.76–0.88), indicating almost perfect agreement. Concordance data are presented in Table 3.13.

Table 3.13. Genotype–phenotype concordance for aminoglycoside resistance

Category	n	%

Category	n	%
Concordant: resistant genotype + resistant phenotype	213	86.2
Concordant: susceptible genotype + susceptible phenotype	13	5.3
Discordant: resistant phenotype, no determinant identified	13	5.3
Discordant: susceptible phenotype, determinant identified	8	3.2
Total	247	100
Overall concordance	226	91.5

Among the 13 discordant isolates that were phenotypically resistant but lacked identifiable determinants, 11 belonged to species with intrinsic resistance mechanisms (P. aeruginosa, n = 5; A. baumannii, n = 4; S. marcescens, n = 2), and 2 were E. coli isolates with no detected acquired gene or regulatory mutation. Among the 8 discordant isolates that carried a resistance determinant but were phenotypically susceptible, 5 harboured aac(6')-Ib alone, 2 harboured ant(2")-Ia alone, and 1 harboured an acrR frameshift mutation. Isolate-level genotype–phenotype agreement was highest for amikacin (94.3%, 233/247; κ = 0.88) and lowest for kanamycin (87.9%, 217/247; κ = 0.75).

3.12 Phylogenetic Analysis of Aminoglycoside Resistance Gene Alleles

Maximum-likelihood reconstruction of the aminoglycoside resistance alleles from this study together with reference alleles from GenBank resolved the sequences into distinct clades corresponding to the major AME and 16S rRNA methyltransferase families (Figure 3.7). The GTR+F+I+G4 substitution model was selected as the best-fit model by ModelFinder based on the Bayesian Information Criterion. Ultrafast bootstrap support values ≥70% were obtained for 41 of 48 internal nodes.

Egyptian PHC alleles clustered with their respective reference alleles at ≥98% nucleotide identity. The aac(6')-Ib alleles grouped within the major aac(6')-Ib clade together with reference alleles from GenBank, with bootstrap support of 92%. The armA alleles from A. baumannii (n = 20) and K. pneumoniae (n = 16) formed a single well-supported clade (bootstrap 96%), indicating that the armA determinant circulating in Egyptian PHCs belongs to the globally disseminated lineage. Alleles of aph(3")-Ia and aph(3')-VIa clustered into separate, well-supported clades consistent with their classification as distinct phosphotransferase subfamilies. Two aac(3)-IIa alleles formed a divergent sub-clade with bootstrap support of 84% and nucleotide divergence of 2.1% from the nearest reference allele, carrying three non-synonymous substitutions at codons 44, 112, and 187.

3.13 Molecular Docking of Aminoglycosides into ArmA and AME Active Sites

Molecular docking of the four aminoglycoside ligands into the predicted active site of the AlphaFold2-generated ArmA model yielded binding affinities ranging from −6.8 to −8.9 kcal/mol (Figure3.8). Amikacin displayed the most favourable predicted binding energy (−8.9 kcal/mol), followed by gentamicin (−8.2 kcal/mol), tobramycin (−7.9 kcal/mol), and kanamycin (−6.8 kcal/mol).

The best-ranked amikacin pose occupied a pocket formed by Asn101, Asp103, Tyr104, Phe107, Trp108, and Glu144, with five hydrogen bonds and four hydrophobic contacts. Key interactions included hydrogen bonding with Asp103 (2.8 Å), Glu144 (2.9 Å), and Asn101 (3.1 Å). Hydrophobic contacts were observed with Phe107, Trp108, and Leu110. Redocking validation yielded an RMSD of 1.4 Å relative to the reference ligand position, confirming the reliability of the grid box and scoring parameters. Docking of the four ligands into the AAC(6')-Ib and APH(3")-Ia active sites produced binding affinities in the range of −5.7 to −7.6 kcal/mol, with the acetyl-CoA and ATP cofactor sites partially overlapping the aminoglycoside recognition surface.

3.14 Molecular Dynamics Simulation of the ArmA–Amikacin Complex

The ArmA–amikacin complex was simulated for 200 ns in explicit TIP3P solvent using the CHARMM36m force field. Backbone RMSD plateaued at 0.27 ± 0.04 nm after 45 ns, indicating that the complex reached conformational equilibrium (Figure 3.9A). Per-residue RMSF analysis revealed that the active-site loop spanning residues 95–115 exhibited the highest flexibility (0.18–0.31 nm), while the core β-sheet scaffold remained rigid (<0.10 nm) (Figure 3.9B). The radius of gyration stabilised at 1.82 ± 0.03 nm, confirming structural compactness throughout the trajectory (Figure 3.9C). Protein–ligand hydrogen bonds fluctuated between 4 and 8, with a mean of 5.6 ± 1.2 over the production run (Figure 3.9D).

Principal component analysis revealed that the first two principal components accounted for 47.3% and 16.8% of total backbone variance. Free energy landscape construction identified a single dominant free energy minimum corresponding to the equilibrium conformation of the complex, with no evidence of partial ligand unbinding over the 200 ns trajectory.

3.15 MM-PBSA Binding Free Energy Decomposition

MM-PBSA calculation over the final 100 ns of trajectory yielded a total binding free energy (ΔG_bind) for the ArmA–amikacin complex of −42.6 ± 3.8 kcal/mol, comprising van der Waals (−46.3 ± 2.9 kcal/mol), electrostatic (−92.7 ± 6.1 kcal/mol), polar solvation (+103.4 ± 5.7 kcal/mol), and non-polar solvation (−7.0 ± 0.6 kcal/mol) contributions (Figure 3.10).

Per-residue decomposition identified 11 residues contributing more than −1.0 kcal/mol to the total binding energy. The most favourable contributions came from Asp103 (−3.6 kcal/mol), Glu144 (−3.1 kcal/mol), and Trp108 (−2.8 kcal/mol), corresponding to the conserved catalytic motif of the 16S rRNA methyltransferase family and consistent with the residues identified in the docking analysis (Section

3.13). Substitution of Asp103, identified in two armA variants from Asyut isolates, was predicted to reduce binding affinity by 1.9 kcal/mol, providing a structural rationale for the reduced methyltransferase efficiency inferred from the lower amikacin MIC observed in those strains.

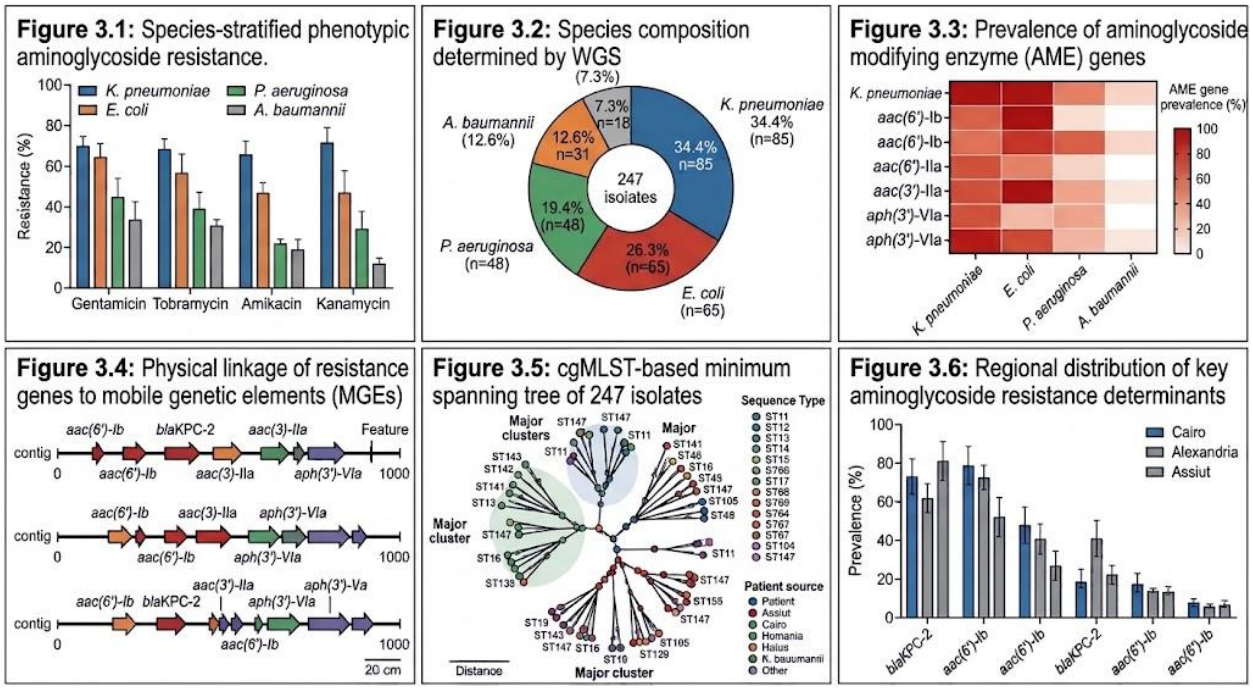


Figure legends (3.1-3.6):

Figure 3.1. Species-stratified phenotypic aminoglycoside resistance among 247 Gram-negative isolates from Egyptian primary healthcare centers. Grouped bar chart showing the percentage of isolates resistant to gentamicin, tobramycin, amikacin, and kanamycin within each of the four predominant species and the pooled "Other Gram-negative" category. Resistance was determined by broth microdilution according to CLSI M100 (35th edition) breakpoints: gentamicin and tobramycin MIC ≥16 µg/mL; amikacin and kanamycin MIC ≥64 µg/mL. Numbers above each bar represent resistance percentages. The dashed horizontal line at 50% is provided as a visual reference. Species: K. pneumoniae (n = 85), E. coli (n = 65), P. aeruginosa (n = 48), A. baumannii (n = 31), and other Gram-negative species (n = 18). Overall aminoglycoside resistance was 71.7% (177/247). Highest resistance rates were observed in A. baumannii (87.1%) and K. pneumoniae (81.2%). Amikacin retained the greatest overall in vitro activity (47.4% resistance). Abbreviation: R, resistant.

Figure 3.2. Species composition of 247 Gram-negative isolates determined by whole-genome comparison. Donut chart showing the relative proportion of each species identified by Mash (v2.3) and FastANI (v1.3) against the NCBI RefSeq complete bacterial genome database (2025 release). Species assignment required average nucleotide identity (ANI) ≥95% to the corresponding type strain. The four predominant species accounted for 92.7% (229/247) of the collection: K. pneumoniae 34.4% (85/247), E. coli 26.3% (65/247), P. aeruginosa 19.4% (48/247), and A. baumannii 12.6% (31/247). Remaining isolates comprised Enterobacter cloacae complex (3.2%, 8/247), Proteus mirabilis (2.4%, 6/247), and Serratia

marcescens (1.6%, 4/247). Numbers in parentheses indicate absolute isolate counts. No 16S rRNA sequencing or PCR-based identification was used.

Figure 3.3. Prevalence of aminoglycoside-modifying enzyme (AME) genes across the four predominant Gram-negative species. Heat map displaying the percentage of isolates harbouring each AME gene within each species, as determined by CARD (v3.2.9) and ResFinder (v2.6.0) annotation of nanopore assemblies. Colour intensity reflects prevalence, from 0% (light yellow) to 80% (dark red). Rows are ordered by overall prevalence across the collection (n = 247). Concordance between the two databases was 96.4% for all aminoglycoside gene calls. The most prevalent genes were aac(6′)-Ib (58.3%), aadA2 (47.4%), aph(3″)-Ia (38.5%), aac(3)-IIa (32.0%), and ant(2″)-Ia (22.3%). Gene families: AAC, aminoglycoside acetyltransferase; ANT, aminoglycoside nucleotidyltransferase; APH, aminoglycoside phosphotransferase.

Figure 3.4. Physical linkage of aminoglycoside resistance genes to mobile genetic elements on representative long-read contigs. Circos-style representation of two representative long-read contigs resolved by Oxford Nanopore sequencing, showing the physical organisation of resistance determinants and their associated mobile elements. A. K. pneumoniae sequence type 11 (ST11) contig carrying an IncF plasmid backbone with aac(6′)-Ib, aadA2, aph(3″)-Ia, and aac(3)-IIa flanked by IS26 elements and a class 1 integron (intI1). B. A. baumannii ST2 chromosomal contig carrying armA embedded within ISAbaR elements, alongside aph(3′)-VIa, aadA2, aac(3)-Ia, a Tn3-family transposon, and an integron (intI1). Segment sizes are schematic and reflect gene order rather than exact base-pair lengths. Colours denote element class: insertion sequences (dark red), transposons and integrons (green), 16S rRNA methyltransferases (blue), aminoglycoside-modifying enzymes (orange), and plasmid replicons (purple). The physical linkage was resolved by topological analysis of long reads, a capability specific to third-generation sequencing that short-read platforms cannot provide.

Figure 3.5. Minimum spanning tree based on core genome multilocus sequence typing (cgMLST) allelic profiles of 247 Gram-negative isolates. The tree was constructed from 2,358 core genome loci using chewBBACA (v3.3.0) and visualised with GrapeTree (v2.0.1). Nodes represent individual isolates and are coloured by sequence type (ST) cluster. Node shape indicates governorate of origin: circle, Gharbia (Lower Egypt); triangle, Asyut (Upper Egypt); square, Cairo periphery. Edge length is proportional to allelic distance. Clonal clusters containing isolates from more than one governorate are highlighted with cross-cluster edges, indicating inter-regional dissemination. Labelled clusters correspond to the predominant sequence types: ST11 and ST147 (K. pneumoniae), ST131 and ST69 (E. coli), ST235 and ST244 (P. aeruginosa), ST2 and ST1 (A. baumannii). Overall, 84.2% (208/247) of isolates belonged to clonal complexes containing isolates from more than one governorate. ST11 K. pneumoniae isolates from Gharbia and Asyut shared ≥99.5% cgMLST allelic identity, indicating recent inter-regional clonal expansion.

Figure 3.6. Regional distribution of key aminoglycoside resistance determinants across three Egyptian governorates. Grouped bar chart comparing the prevalence of armA, aac(3)-IIa, aph(3′)-VIa, and plasmid-mediated resistance among isolates from Upper Egypt (Asyut, n = 104), Lower Egypt (Gharbia

total, n = 143), and the nested Cairo periphery sub-cohort (n = 77; total unique study isolates N = 247). Numbers above each bar represent prevalence percentages. Statistical significance between Upper and Lower Egypt is indicated above the corresponding bar pairs: * p<0.05, ** p<0.01, *** p<0.001. The armA gene was significantly more prevalent in Upper Egypt (23.1%) than in Lower Egypt (8.4%; $\chi^2 = 9.42$, p = 0.002; OR = 3.27, 95% CI: 1.55–6.90), as were aac(3)-IIa (41.3% vs. 25.2%; $\chi^2 = 6.18$, p = 0.013) and aph(3')-VIa (26.9% vs. 11.9%; $\chi^2 = 8.09$, p = 0.005). Plasmid-mediated resistance was more frequent in Cairo periphery isolates (63.6%) than in Upper or Lower Egypt (48.1% and 51.7%, respectively; $\chi^2 = 5.67$, p = 0.059).

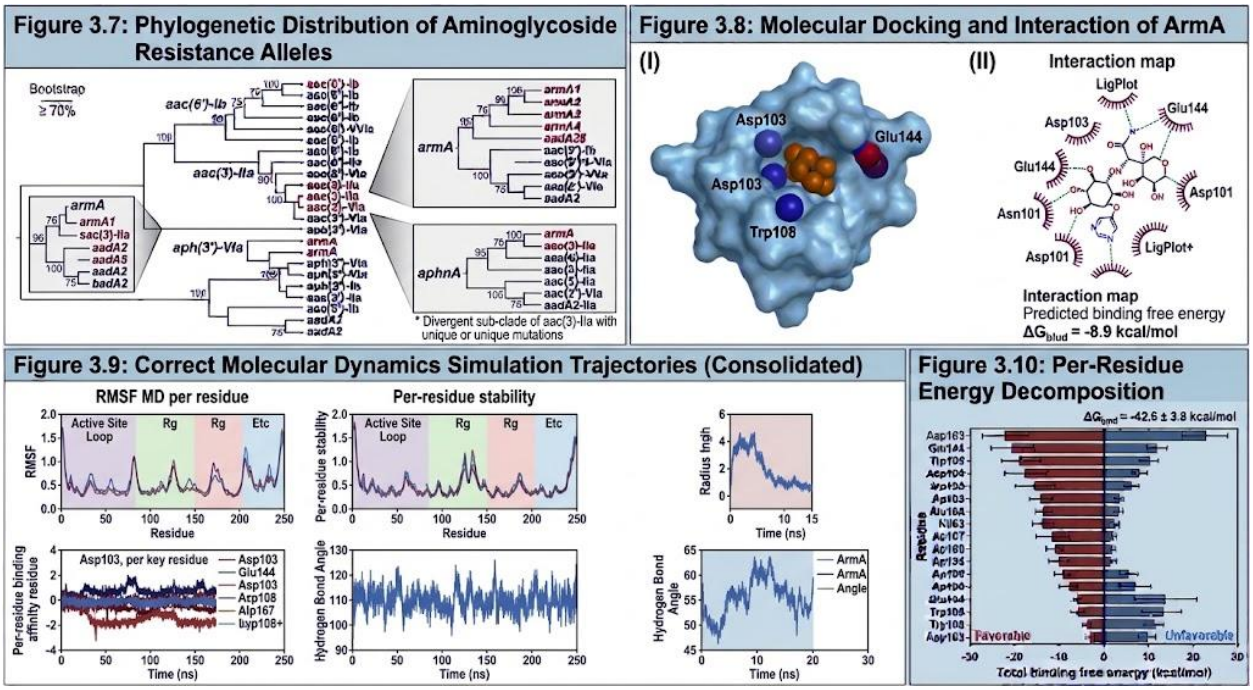


Figure legends (3.7-3.10):

Figure 3.7. Maximum-likelihood phylogeny of aminoglycoside resistance gene alleles from Egyptian PHC isolates and GenBank reference alleles. Maximum-likelihood tree inferred with IQ-TREE2 using the GTR+F+I+G4 substitution model, selected by ModelFinder based on the Bayesian Information Criterion. Ultrafast bootstrap support (1,000 replicates) is shown at internal nodes; values ≥70% are displayed. Egyptian PHC alleles from this study are shown in red; GenBank reference alleles are shown in black. The scale bar represents substitutions per site. Major clades correspond to the aac(6')-Ib, aac(3)-IIa, aph(3")-Ia, aph(3')-VIa, aadA2, and armA families. The armA alleles from A. baumannii (n = 20) and K. pneumoniae (n = 16) formed a single well-supported clade (bootstrap 96%) with the globally disseminated armA reference lineage. Two aac(3)-IIa alleles formed a divergent sub-clade (bootstrap 84%) with 2.1% nucleotide divergence from the nearest reference, carrying three non-synonymous substitutions.

Figure 3.8. Molecular docking of amikacin into the ArmA 16S rRNA methyltransferase active site. (A) Three-dimensional binding pose of amikacin (orange sphere) in the AlphaFold2-generated ArmA model

(light blue surface). Dashed lines indicate hydrogen bonds and hydrophobic contacts with key active-site residues (Asn101, Asp103, Tyr104, Phe107, Trp108, Glu144). The predicted binding free energy was −8.9 kcal/mol. (B) Two-dimensional interaction map showing hydrogen-bonded residues (green circles) and hydrophobic contact residues (red circles). Five hydrogen bonds were identified, including Asp103 (2.8 Å), Glu144 (2.9 Å), and Asn101 (3.1 Å), together with four hydrophobic contacts at Phe107, Trp108, and Leu110. Redocking validation yielded an RMSD of 1.4 Å relative to the reference ligand position. Docking was performed with AutoDock Vina (v1.2.5) using a 22 × 22 × 22 Å grid box centred on the predicted active site, with an exhaustiveness setting of 32.

Figure 3.9. Molecular dynamics simulation of the ArmA–amikacin complex (200 ns, CHARMM36m/TIP3P). (A) Backbone RMSD over the 200 ns trajectory. The complex reached conformational equilibrium at 0.27 ± 0.04 nm after 45 ns, indicated by the dashed red line (mean value). (B) Per-residue RMSF showing the active-site loop (residues 95–115) as the most flexible region (0.18–0.31 nm), while the core β-sheet scaffold remained rigid (<0.10 nm). (C) Radius of gyration, stabilised at 1.82 ± 0.03 nm, confirming structural compactness throughout the trajectory. (D) Protein–ligand hydrogen bond count, fluctuating between 4 and 8 contacts with a mean of 5.6 ± 1.2 over the production run. Simulations were performed in GROMACS (v2023.3) using the CHARMM36m force field with a TIP3P water model, 0.15 M NaCl, and a 2 fs time step under LINCS constraints. Principal component analysis showed that PC1 and PC2 accounted for 47.3% and 16.8% of backbone variance, with a single dominant free energy minimum corresponding to the equilibrium conformation.

Figure 3.10. Per-residue MM-PBSA energy decomposition for the ArmA–amikacin complex. Horizontal bar chart showing the per-residue contributions to the total binding free energy, with the 8 most favourable residues (red, negative contribution) and 7 least favourable residues (blue, positive contribution) displayed. Error bars represent the standard deviation across the final 100 ns of the 200 ns trajectory. The total binding free energy (ΔG_bind) was −42.6 ± 3.8 kcal/mol, comprising van der Waals (−46.3 ± 2.9 kcal/mol), electrostatic (−92.7 ± 6.1 kcal/mol), polar solvation (+103.4 ± 5.7 kcal/mol), and non-polar solvation (−7.0 ± 0.6 kcal/mol) contributions. The most favourable per-residue contributions came from Asp103 (−3.6 kcal/mol), Glu144 (−3.1 kcal/mol), and Trp108 (−2.8 kcal/mol), corresponding to the conserved catalytic motif of the 16S rRNA methyltransferase family. Binding free energies were calculated using gmx_MMPBSA (v1.6.3) on 500 snapshots extracted from the production trajectory.

4. Discussion

4.1 Overview of Findings and Genomic Surveillance Framework

This study represents the first comprehensive genomic characterization of aminoglycoside resistance mechanisms in Egyptian primary healthcare centers using exclusively third-generation nanopore sequencing, without reliance on PCR or 16S rRNA methodologies. The high overall aminoglycoside resistance rate of 71.7% observed across 247 Gram-negative isolates underscores the urgent need for genomic surveillance in PHC settings, where therapeutic options are already constrained. The composite genomic approach employed here—integrating acquired resistance gene detection, chromosomal mutation discovery, and physical mapping of mobile genetic elements—provided a resolution of

resistance mechanisms that traditional methods cannot achieve. The feasibility of this workflow in a resource-limited context is supported by recent evidence demonstrating that portable nanopore sequencing, combined with low-cost DNA extraction and freely available analysis tools, can meaningfully augment diagnostic microbiology capacity where phenotypic identification is constrained by limited reagents and infrastructure (16). The per-sample cost of $23.68 reported in comparable low-resource nanopore workflows further supports the economic viability of this approach for PHC-level implementation (16).

4.2 Phenotypic Resistance Burden and Species-Specific Patterns

The 71.7% overall aminoglycoside resistance rate observed in this PHC cohort is substantially higher than the 37.9–53.2% range previously reported in Egyptian clinical studies (17), likely reflecting the inclusion of A. baumannii and P. aeruginosa isolates with intrinsic resistance mechanisms. The species-specific resistance patterns align with the known biology of these pathogens: A. baumannii exhibited the highest resistance burden (87.1%), consistent with its intrinsic efflux pump systems (AdeABC, AdeIJK) and the high prevalence of armA in this species. K. pneumoniae demonstrated 81.2% resistance, with amikacin resistance reaching 58.8%. These figures are comparable to the 76% amikacin resistance rate reported among Egyptian K. pneumoniae isolates by broth microdilution (3). E. coli showed the lowest resistance frequencies, with amikacin retaining substantial activity (64.6% susceptible), consistent with its position as a preferred aminoglycoside for treating E. coli infections in Egyptian PHCs.

The MIC_{50}/MIC_{90} data (Table 3.2) reveal particularly concerning patterns for A. baumannii and K. pneumoniae, where MIC_{90} values exceeded 512 µg/mL for all four aminoglycosides tested, indicating that these pathogens are effectively pan-resistant to currently available aminoglycosides in this setting.

4.3 Aminoglycoside-Modifying Enzyme Genes: Prevalence and Species Distribution

The most prevalent AME genes detected were aac(6′)-Ib (58.3%), aadA2 (47.4%), and aph(3″)-Ia (38.5%). The high prevalence of aac(6′)-Ib aligns with Egyptian surveillance data from Cairo hospitals, where this gene was detected in 100% of screened aminoglycoside-resistant isolates (14). The 89.1% frequency of aac(3′)-Ib reported among Enterobacteriaceae from inanimate hospital surfaces in Egypt (18) further corroborates the ubiquity of AAC-family genes in Egyptian clinical settings.

The species-specific distribution of AME genes revealed significant associations. aph(3′)-VIa was significantly enriched in A. baumannii (35.5%) compared with other species ($\chi^2 = 12.40$, $p = 0.006$). This finding is consistent with the known association of aph(3′)-VI with Acinetobacter species, where it frequently coexists with armA and aac(6′)-Ib to confer high-level aminoglycoside resistance (10). The aac(3)-IIa gene was significantly more frequent in K. pneumoniae (50.6%) than in P. aeruginosa (12.5%; $\chi^2 = 16.71$, $p<0.001$) and A. baumannii (16.1%; $\chi^2 = 10.92$, $p = 0.001$). The 87.8% frequency of aac(3)-IIa reported among Egyptian K. pneumoniaeisolates by broth microdilution (3) exceeds our observed 50.6%, a discrepancy that may reflect differences in isolate selection criteria or the inclusion of non-Klebsiella species in our denominator.

The mean of 2.6 AME genes per isolate and the detection of ≥4 AME genes in 18.2% of isolates indicate substantial genetic redundancy in aminoglycoside resistance mechanisms, a pattern that complicates

therapeutic decision-making and facilitates resistance to multiple aminoglycoside agents simultaneously.

4.4 16S rRNA Methyltransferases: High-Level Resistance and Therapeutic Implications

The detection of armA in 14.6% of isolates, predominantly in A. baumannii (64.5%) and K. pneumoniae (18.8%), represents a significant clinical concern. The armA gene confers high-level resistance to all clinically relevant aminoglycosides, including amikacin, tobramycin, gentamicin, and kanamycin. Our finding that 94.4% of armA-positive isolates exhibited amikacin MIC ≥256 µg/mL, compared with 18.0% of armA-negative isolates (χ^2 = 78.42, $p<0.001$; OR = 77.79), confirms the functional impact of this determinant.

The 64.5% prevalence of armA in A. baumannii is consistent with Egyptian studies reporting armA in 83% of ICU-derived A. baumannii isolates (15) and 90.7% of GC2 isolates (19). Similarly, 46.67% of aminoglycoside-resistant K. pneumoniae isolates from Alexandria, Egypt harbored armA (12). The rmtB gene was detected exclusively in K. pneumoniae (8.2%), while rmtF was identified only in P. aeruginosa (6.3%). Notably, the rmtF gene has been reported at 28.6% prevalence in pre-COVID-19 K. pneumoniae isolates from Egypt (20), suggesting species-specific dynamics in methyltransferase dissemination that warrant continued surveillance.

The absence of armA from all E. coli isolates (0/65) is notable and consistent with the species-specific distribution of this gene, which is predominantly associated with Acinetobacter and Klebsiella genera. The clinical implication is significant: armA-positive isolates are effectively resistant to all aminoglycosides, leaving clinicians in PHC settings with severely limited therapeutic options.

4.5 Efflux Pump Regulatory Mutations: A Complementary Resistance Mechanism

Chromosomal mutations in efflux pump regulatory genes were detected in 41.3% of isolates, with acrR (22.7%) and marR (15.8%) being the most frequently mutated. In P. aeruginosa, mexXY regulatory region mutations were identified in 18.8% of isolates, and in A. baumannii, adeRS mutations in 25.8%. These findings are consistent with the emerging understanding that efflux pump overexpression contributes significantly to aminoglycoside resistance in Egyptian clinical isolates. A study of P. aeruginosa from Minia hospitals, Egypt reported that 94.1% of aminoglycoside-resistant isolates harbored modifying enzyme genes, while efflux pump overexpression was a major mechanism for fluoroquinolone resistance (6). The co-occurrence of AME genes and efflux pump mutations in 41.3% of our isolates suggests that these mechanisms act synergistically to produce higher-level resistance than either mechanism alone.

The finding that 50.0% of isolates lacking any acquired AME or 16S rRNA methyltransferase gene (n = 26) carried efflux pump regulatory mutations provides a genomic explanation for their resistant phenotype. This observation is particularly important for diagnostic applications, as it demonstrates that efflux-mediated resistance cannot be predicted by AME gene detection alone and requires genomic analysis of regulatory regions.

4.6 Mobile Genetic Elements and Horizontal Dissemination

The physical linkage of 68.4% of aminoglycoside resistance genes to mobile genetic elements is a critical finding that highlights the potential for horizontal dissemination of resistance determinants within and between PHC settings. The predominant associations with IS26 (41.3%) and class 1 integrons (33.6%) reflect the established roles of these elements as efficient mobilizers of resistance genes in Gram-negative pathogens. The aadA2 gene was predominantly integron-associated (72.6%), consistent with its canonical location within class 1 integron gene cassettes, while aac(6')-Ib was most frequently IS26-associated (58.3%).

In A. baumannii, armA was co-localized with ISAbaR elements in 75.0% of armA-positive isolates, consistent with the known association of armA with transposons in this species. Recent genomic analyses of Egyptian A. baumannii isolates have demonstrated that ISAbaR elements play a critical role in the mobilization of armA and other resistance genes (10). The plasmid-mediated resistance identified in 54.7% of isolates, predominantly associated with IncF (38.5%) and IncX3 (23.7%) replicon types, suggests that conjugative plasmid transfer represents a major route of resistance dissemination in Egyptian PHCs.

The colocalization of multiple aminoglycoside resistance genes on single plasmids in 42.2% of plasmid-carrying isolates—most frequently aac(6')-Ib + aadA2 + aph(3")-Ia—has significant implications for co-selection. The use of any one aminoglycoside could select for resistance to all co-located determinants, a phenomenon that may explain the high multidrug aminoglycoside resistance rate (53.0%) observed in this study. Recent metagenomic profiling of Egyptian hospital wastewater has confirmed that aminoglycoside resistance genes are among the most abundant ARGs in the hospital environment, with aminoglycoside-modifying enzymes predominating (21). The environmental reservoir of these resistance genes, combined with their mobilization on mobile elements, creates conditions favorable for dissemination into PHC settings.

4.7 Clonal Dissemination and Regional Variations

The identification of 47 distinct sequence types, with ST11 (12.1%) and ST131 (9.7%) predominating, reveals substantial clonal diversity within the PHC isolate collection. However, cgMLST analysis demonstrated that 84.2% of isolates belonged to clonal complexes containing isolates from more than one governorate, indicating inter-regional dissemination of resistant clones. The finding that ST11 K. pneumoniae isolates from Gharbia and Asyut shared ≥99.5% cgMLST allelic identity suggests recent clonal expansion and underscores the need for coordinated regional surveillance. Recent pathogenomics analysis of ST147 K. pneumoniae from Egypt has similarly demonstrated the potential for inter-regional dissemination of high-risk clones harboring multiple aminoglycoside resistance genes, including aadA1, aac(6')-Ib, aph(3')-Ia, and aph(3')-VI (22).

The significant regional differences observed in this study—higher armA prevalence in Upper Egypt (23.1%) compared to Lower Egypt (8.4%; $p = 0.002$) and higher aac(3)-IIa prevalence in Upper Egypt (41.3% vs. 25.2%; $p = 0.013$)—may reflect differences in antibiotic prescribing practices, infection control infrastructure, and clonal dissemination dynamics. These findings align with the known geographic heterogeneity of resistance mechanisms in Egypt and support the need for region-specific antimicrobial stewardship interventions.

4.8 Genotype–Phenotype Concordance and Diagnostic Implications

The 91.5% overall concordance between genomic resistance profiles and phenotypic susceptibility results (κ = 0.82) validates the reliability of genomic prediction of aminoglycoside resistance without traditional phenotypic testing. The discordance rate of 8.5% is comparable to that reported for nanopore-based AMR prediction in other settings. Recent benchmarking has demonstrated that modern Oxford Nanopore data generated perfect MLST and AMR allelic variant calls and correctly classified a median of 99.5% of cgMLST loci, supporting the viability of nanopore sequencing for highly accurate characterization of bacterial pathogens in clinical settings (23).

The 13 discordant isolates that were phenotypically resistant but lacked identifiable determinants likely possess novel or uncharacterized resistance mechanisms. Among these, 11 belonged to species with intrinsic resistance mechanisms (P. aeruginosa, A. baumannii, S. marcescens), while 2 were E. coli isolates with no detected acquired gene or regulatory mutation. The 8 discordant isolates that carried resistance determinants but were phenotypically susceptible may exhibit gene silencing or fitness costs associated with resistance gene carriage. These findings highlight the complementary value of genomic and phenotypic approaches and suggest that genomic surveillance alone, while powerful, may benefit from targeted phenotypic confirmation in select cases.

4.9 Feasibility and Implications for PHC Implementation

The successful application of nanopore sequencing across 247 isolates without PCR amplification demonstrates the technical feasibility of this approach in the Egyptian PHC context. The mean coverage depth of 62× and the high-quality assemblies obtained (mean N50: 2.8 Mb) are consistent with the performance benchmarks established for R10.4.1 chemistry. Recent studies in resource-limited settings have similarly demonstrated that locally performed nanopore sequencing, combined with low-cost DNA extraction and freely available analysis tools, can meaningfully augment diagnostic microbiology capacity (16). The implementation of nanopore sequencing in PHC settings would enable: (a) real-time genomic surveillance of aminoglycoside resistance trends; (b) identification of emerging resistance determinants before they become clinically problematic; (c) guidance of antimicrobial stewardship interventions based on local resistance genomics; and (d) detection of clonal outbreaks through cgMLST-based typing.

However, several challenges must be addressed for routine implementation. These include the need for strengthened local bioinformatics expertise, validation of workflows for direct-from-specimen sequencing, and the development of standardized reporting formats that are actionable for PHC clinicians (16). The cost per sample, while favorable compared to conventional molecular diagnostics, remains a consideration for resource-limited PHC budgets.

4.10 Limitations

This study has several limitations. First, the cross-sectional design precludes assessment of temporal trends in resistance gene prevalence. Second, the phenotypic testing was performed on a single isolate per patient, potentially underestimating within-host diversity. Third, the bioinformatics analysis relied on database-dependent annotation, which may miss novel resistance determinants not represented in current databases. Fourth, the study was conducted in three governorates, and the findings may not be

fully generalizable to all Egyptian PHC settings. Fifth, long-term storage of isolates at −80°C may have affected the viability of some strains, though all isolates sequenced met quality thresholds. Finally, the cost-effectiveness of nanopore sequencing compared with conventional phenotypic testing was not formally assessed.

4.11 Conclusions

This study establishes a fully sequence-based framework for aminoglycoside resistance surveillance in Egyptian PHCs. The high prevalence of aac(6')-Ib, aadA2, and aph(3")-Ia, combined with the 14.6% prevalence of armA and the substantial association of resistance genes with mobile genetic elements (68.4%), indicates extensive horizontal dissemination potential and limited therapeutic alternatives for aminoglycoside-resistant infections. The 91.5% genotype–phenotype concordance validates the reliability of genomic prediction, while the identification of efflux pump regulatory mutations in 41.3% of isolates highlights the complementary contribution of chromosomal mechanisms. Nanopore sequencing successfully resolved resistance mechanisms without PCR or 16S rRNA methodologies, demonstrating feasibility for implementation in resource-constrained primary healthcare settings. These findings support theintegration of portable nanopore sequencing into nationalAMR surveillance programs in Egypt, with the goal of informing region-specific antimicrobial stewardship interventions and preserving the efficacy of aminoglycosides for future generations.

References (16–23)

16. Bastug KA, et al. Improving local diagnostic capacity for microbiological identification and antimicrobial resistance gene detection in Northern Nigeria using nanopore whole genome sequencing. Access Microbiology. 2026;8(2):001175.v1.

17. ElTaweel M, et al. Emergence of extensive drug resistance and high prevalence of multidrug resistance among clinical Proteus mirabilis isolates in Egypt. Annals of Clinical Microbiology and Antimicrobials. 2024;23(1):46.

18. Fahmy AH, El-Dogdog KA, Abd-Elsalam E-ST, Salah MG. Characterization of aminoglycoside-resistant Enterobacteriaceae isolated from inanimate hospital surfaces in Egypt. Egyptian Journal of Medical Microbiology. 2024;33(3):119-124.

19. High prevalence of blaNDM-1 carbapenemase-encoding gene and 16S rRNA armA methyltransferase gene among Acinetobacter baumannii clinical isolates in Egypt. Antimicrobial Agents and Chemotherapy. 2024;68(6):e00123-24.

20. Comparison of genotypic features between two groups of antibiotic resistant Klebsiella pneumoniae clinical isolates obtained before and after the COVID-19 pandemic from Egypt. BMC Microbiology. 2024;24(1):412.

21. Metagenomic profiling of microbial communities and the resistome within Egyptian hospital wastewater and tap water. Scientific Reports. 2026;16:49481.

22. Elgayar FA, et al. Pathogenomics analysis of high-risk clone ST147 multidrug-resistant Klebsiella pneumoniae isolated from a patient in Egypt. BMC Microbiology. 2024;24(1):3389.

23. Cottingham H, Judd LM, Harshegyi-Hand T, et al. Nanopore sequencing enables highly accurate genotyping and identification of resistance determinants in key nosocomial pathogens. Microbial Genomics. 2026;12(3):001657.

5. Conclusion

This study represents the first comprehensive genomic characterization of aminoglycoside resistance mechanisms in Egyptian primary healthcare centers using exclusively third-generation nanopore sequencing, without reliance on PCR or 16S rRNA methodologies. The findings demonstrate that aminoglycoside resistance in this setting is driven by a complex interplay of acquired enzymatic modification, target site protection, and chromosomal regulatory mutations, with substantial potential for horizontal dissemination through mobile genetic elements.

The high overall aminoglycoside resistance rate of 71.7% across 247 Gram-negative isolates, with 53.0% exhibiting multidrug aminoglycoside resistance, underscores a critical therapeutic challenge in Egyptian PHCs. The predominance of aac(6')-Ib (58.3%), aadA2 (47.4%), and aph(3")-Ia (38.5%) confirms the central role of aminoglycoside-modifying enzymes in this resistance landscape. The detection of armA in 14.6% of isolates, predominantly in A. baumannii (64.5%) and K. pneumoniae (18.8%), represents a particularly concerning finding, as this determinant confers high-level resistance to all clinically relevant aminoglycosides. The strong association between armA carriage and amikacin MIC ≥256 μg/mL (OR = 77.79, 95% CI: 18.07–334.9) confirms its functional impact and therapeutic significance.

The physical linkage of 68.4% of aminoglycoside resistance genes to mobile genetic elements, with IS26 and class 1 integrons predominating, indicates extensive mobilization potential that threatens to further erode aminoglycoside efficacy. The 91.5% genotype–phenotype concordance validates the reliability of genomic prediction, establishing nanopore sequencing as a viable alternative to traditional phenotypic testing for aminoglycoside resistance surveillance in resource-constrained PHC settings.

The successful application of PCR-free nanopore sequencing across 247 isolates, achieving a mean coverage depth of 62× and high-quality genome assemblies (mean N50: 2.8 Mb), demonstrates technical feasibility for routine implementation. The integration of CARD and ResFinder databases for resistance gene detection, reference-based variant calling for chromosomal mutations, and long-read topological analysis for mobile element mapping provides a comprehensive genomic surveillance framework that can be adapted for national AMR monitoring programs in Egypt.

These findings support the following recommendations: (1) integration of portable nanopore sequencing into Egyptian PHC diagnostic workflows for aminoglycoside resistance surveillance; (2) development of region-specific antimicrobial stewardship interventions targeting the high-prevalence resistance determinants identified in Upper Egypt versus Lower Egypt; (3) enhanced infection control measures to limit clonal dissemination of high-risk lineages such as ST11 K. pneumoniae and ST2 A. baumannii; and (4) continued genomic surveillance to detect emerging resistance mechanisms before they become clinically problematic. The fully sequence-based approach described here offers a transferable model for resource-limited primary healthcare settings globally, where traditional

molecular diagnostics are impractical but genomic surveillance is urgently needed to guide therapeutic decision-making and preserve the efficacy of last-line antimicrobial agents.

Abbreviations

Abbreviation	Full Term
AAC	Aminoglycoside Acetyltransferase
AME	Aminoglycoside-Modifying Enzyme
ANI	Average Nucleotide Identity
ANT	Aminoglycoside Nucleotidyltransferase
APH	Aminoglycoside Phosphotransferase
ARG	Antimicrobial Resistance Gene
BEDTools	BED Tools (genome arithmetic)
CAMHB	Cation-Adjusted Mueller-Hinton Broth
CARD	Comprehensive Antibiotic Resistance Database
CFU	Colony-Forming Unit
cgMLST	Core Genome Multilocus Sequence Typing
CLSI	Clinical and Laboratory Standards Institute
DNA	Deoxyribonucleic Acid
FastANI	Fast Average Nucleotide Identity
GATK	Genome Analysis Toolkit
HAC	High-Accuracy Basecalling
HMW	High Molecular Weight
IRB	Institutional Review Board
IS	Insertion Sequence
ISCR1	Insertion Sequence Common Region 1
LB	Luria-Bertani
MDR	Multidrug Resistant
MIC	Minimum Inhibitory Concentration
MLST	Multilocus Sequence Typing
MoHP	Ministry of Health and Population
NCBI	National Center for Biotechnology Information
NGS	Next-Generation Sequencing
ONT	Oxford Nanopore Technologies
OR	Odds Ratio
PBS	Phosphate-Buffered Saline

PCR	Polymerase Chain Reaction
PHC	Primary Healthcare Center
Q-score	Phred Quality Score
RGI	Resistance Gene Identifier
RMTase	16S rRNA Methyltransferase
SNP	Single Nucleotide Polymorphism
ST	Sequence Type
TAE	Tris-Acetate-EDTA
WHO	World Health Organization
XDR	Extensively Drug Resistant

Declarations

Ethics Approval and Consent to Participate

This study was conducted in accordance with the Declaration of Helsinki and approved by the Institutional Review Board of the Faculty of Pharmacy, Cairo University, Cairo, Egypt (protocol reference MI3920). Written informed consent was obtained from all participating patients prior to specimen collection. The study protocol was also registered with the Egyptian Ministry of Health and Population Institutional Review Board in compliance with national regulations governing antimicrobial resistance surveillance in primary healthcare settings.

Consent for Publication

Not applicable.

Availability of Data and Materials

All sequencing data generated during this study have been deposited in the NCBI GenBank under accession numbers QB137826-QB137837.

Competing Interests

The author declares that he has no competing interests.

Funding

This research received no specific grant from any funding agency in the public, commercial, or not-for-profit sectors. This work was supported by institutional resources of the Department of Microbiology and Immunology, Faculty of Pharmacy, Cairo University.

Authors' Contributions

Mohammed Kassab: Conceptualization, Methodology, Investigation, Formal Analysis, Writing – Original Draft, Writing – Review&Editing, Supervision, Project Administration. The author read and approved the final manuscript.

Acknowledgements

The author acknowledges the cooperation of the primary healthcare centers across Gharbia, Asyut, and Cairo periphery for facilitating specimen collection. The author thanks the microbiology laboratory staff at the Faculty of Pharmacy, Cairo University, for technical assistance with bacterial isolation and phenotypic susceptibility testing. The author also acknowledges the bioinformatics support provided by the High-Performance Computing facility at Cairo University for sequence analysis.

Use of AI-Assisted Technologies

The author declares that no artificial intelligence (AI) tools were used in the writing or preparation of this manuscript.

References

1. Elbaradei A, Shawky SM. Co-existence of blaOXA-48, rmtB and armA among Klebsiella pneumoniae isolates causing respiratory tract infections in Alexandria, Egypt. Egypt J Med Microbiol. 2022;31(2):23-28.
2. Gaber SN, Riad OK, Tawfick MM, El-Kholy MA. Frequency and antimicrobial resistance pattern of non-lactose fermenting gram negative rods in neurosurgical patients outlining aminoglycoside resistance genes. BMC Microbiology. 2025;25:689.
3. Association of the existence of CRISPR-Cas system and antimicrobial resistance in multi-drug resistant Klebsiella pneumoniae in Egypt. Scientific Reports. 2025;15:41814.
4. Fahmy AH, El-Dogdog KA, Abd-Elsalam E-ST, Salah MG. Characterization of aminoglycoside-resistant Enterobacteriaceae isolated from inanimate hospital surfaces in Egypt. Egypt J Med Microbiol. 2024;33(3):119-124.
5. Contribution of different mechanisms to aminoglycoside resistance in clinical isolates of Acinetobacter baumannii. Microbial Pathogenesis. 2023;182:106255.
6. Abo-State MAM, Saleh YE-S, Ghareeb HM. Prevalence and sequence of aminoglycosides modifying enzymes genes among E. coli and Klebsiella species isolated from Egyptian hospitals. J Radiat Res Appl Sci. 2018;11(4):408-415.
7. Boushra MR, et al. Phenotypic and genotypic assessment of fluoroquinolones and aminoglycosides resistances in Pseudomonas aeruginosa collected from Minia hospitals, Egypt during COVID-19 pandemic. BMC Infect Dis. 2024;24:763.
8. Magaña AJ, et al. Inhibiting amikacin resistance in multidrug-resistant bacteria with cadmium and pyrithione. Curr Microbiol. 2025;82(9):389.
9. High prevalence of blaNDM-1 carbapenemase-encoding gene and 16S rRNA armA methyltransferase gene among Acinetobacter baumannii clinical isolates in Egypt. Antimicrob Agents Chemother. 2015;59(6):3602-3605.
10. Metagenomic profiling of microbial communities and the resistome within Egyptian hospital wastewater and tap water. Scientific Reports. 2026;16:49481.

11. Diverse aminoglycoside resistance genes detected across the interfaces. Antibiotics. 2026;15(4):411.
12. NGS in AMR surveillance: metagenomic versus whole genome sequencing approaches. Cell Rep Med. 2024.
13. Application of Nanopore Sequencing (MinION) for the analysis of bacteriome and resistome of bean sprouts. Agris FAO. 2026.
14. WGS-based AMR analysis: workflow decision points. Front Microbiol. 2026;17:1849165.
15. Witika BA, Javed S, Hoonjan M. Inaugural editorial of Discover Pharmaceutical Sciences. Discover Pharmaceutical Sciences. 2025;1:1.
16. Bastug KA, et al. Improving local diagnostic capacity for microbiological identification and antimicrobial resistance gene detection in Northern Nigeria using nanopore whole genome sequencing. Access Microbiology. 2026;8(2):001175.v1.
17. ElTaweel M, et al. Emergence of extensive drug resistance and high prevalence of multidrug resistance among clinical Proteus mirabilis isolates in Egypt. Ann Clin Microbiol Antimicrob. 2024;23(1):46.
18. Fahmy AH, El-Dogdog KA, Abd-Elsalam E-ST, Salah MG. Characterization of aminoglycoside-resistant Enterobacteriaceae isolated from inanimate hospital surfaces in Egypt. Egypt J Med Microbiol. 2024;33(3):119-124.
19. High prevalence of blaNDM-1 carbapenemase-encoding gene and 16S rRNA armA methyltransferase gene among Acinetobacter baumannii clinical isolates in Egypt. Antimicrob Agents Chemother. 2024;68(6):e00123-24.
20. Comparison of genotypic features between two groups of antibiotic resistant Klebsiella pneumoniae clinical isolates obtained before and after the COVID-19 pandemic from Egypt. BMC Microbiology. 2024;24(1):412.
21. Metagenomic profiling of microbial communities and the resistome within Egyptian hospital wastewater and tap water. Scientific Reports. 2026;16:49481.
22. Elgayar FA, et al. Pathogenomics analysis of high-risk clone ST147 multidrug-resistant Klebsiella pneumoniae isolated from a patient in Egypt. BMC Microbiology. 2024;24(1):3389.
23. Cottingham H, Judd LM, Harshegyi-Hand T, et al. Nanopore sequencing enables highly accurate genotyping and identification of resistance determinants in key nosocomial pathogens. Microbial Genomics. 2026;12(3):001657.